J. Fluid Mech. (1996), *vol.* 324, *pp.* 223–259

Bioconvection in suspensions of oxytactic bacteria: linear theory

By A. J. HILLESDON AND T. J. PEDLEY†
Department of Applied Mathematical Studies, University of Leeds, Leeds LS2 9JT, UK

(Received 31 January 1995 and in revised form 12 January 1996)

When a suspension of the bacterium *Bacillus subtilis* is placed in a chamber with its upper surface open to the atmosphere, complex bioconvection patterns form. These arise because the cells (*a*) are denser than water, and (*b*) swim upwards on average so that the density of an initially uniform suspension becomes greater at the top than at the bottom. When the vertical density gradient becomes large enough an overturning instability occurs which evolves ultimately into the observed patterns. The cells swim upwards because they are oxytactic, i.e. they swim up gradients of oxygen, and they consume oxygen. These properties are incorporated in conservation equations for the cell and oxygen concentrations, which, for the pre-instability stage of the pattern formation process, have been solved in a previous paper (Hillesdon, Pedley & Kessler 1995). In this paper we carry out a linear instability analysis of the steady-state cell and oxygen concentration distributions. There are intrinsic differences between the shallow- and deep-chamber cell concentration distributions, with the consequence that the instability is non-oscillatory in shallow chambers, but must be oscillatory in deep chambers whenever the critical wavenumber is non-zero. We investigate how the critical Rayleigh number for the suspension varies with the three independent parameters of the problem and discuss the most appropriate definition of the Rayleigh number. Several qualitative aspects of the solution of the linear instability problem agree with experimental observation.

1. Introduction

1.1. *The physical mechanism for bioconvection*

When a suspension of bacterial cells of the species *Bacillus subtilis* is placed in a chamber with its upper surface open to the atmosphere, complex bioconvection patterns are observed (Kessler 1989). These arise because the cells (*a*) are denser than water and (*b*) swim upwards on average so that the density of an initially uniform suspension becomes greater at the top than the bottom. When the vertical density gradient becomes large enough, an overturning instability occurs which evolves ultimately into the observed patterns. The cells swim upwards because they are oxytactic, i.e. they swim up gradients of oxygen (which are initially vertical); the oxygen gradients form because the cells consume oxygen, but the oxygen concentration (C) has the atmospheric value C_0 at the free surface. These properties are incorporated in conservation equations for C and the cell concentration (N) which, together with the Navier–Stokes and mass conservation equations of hydrodynamics, form a continuum model of the suspension. The solution of the cell and oxygen conservation equations in conditions when the fluid velocity is zero and N and C depend only on the vertical

† Present address: Department of Applied Mathematics and Theoretical Physics, University of Cambridge, Silver Street, Cambridge CB3 9EW, UK.

coordinate and time, was given by Hillesdon, Pedley & Kessler (1995, referred to hereinafter as HPK). Here we analyse the linear instability of the steady-state solutions predicted in that paper. Where possible, analytical solutions are given, but in general the problem must be solved numerically. The aim of the work is to determine conditions at the onset of instability and their dependence on the model parameters.

The suspension is taken to occupy a chamber of depth h. It is supposed that the steady-state cell and oxygen concentration distributions have developed from an initial condition in which the suspension was well-mixed, i.e. N and C were uniform. There is an upper free surface so that oxytaxis causes an unstable, densely packed cell layer to form at the top, beneath which the chamber is significantly depleted of cells. For sufficiently large depths, a stable zone of inactive cells arises near the bottom of the chamber; the effect of this on the overall stability of the suspension is of particular interest.

1.2. *The continuum model*

We suppose each cell to have volume v and density ρ_c, such that $\rho_c > \rho_w$, where ρ_w is the density of the watery medium in which the cells swim, and $(\rho_c - \rho_w)/\rho_w \ll 1$. This ensures that the cells are only slightly denser than water. The number of cells in a small volume $\Delta\Omega$, centred at a point $\boldsymbol{X}$, is $N(\boldsymbol{X}, T)\,\Delta\Omega$, where $\boldsymbol{X}$ is measured relative to rectangular Cartesian axes $OXYZ$ with the Z-axis vertically down, and T is the time. The suspension is assumed to be dilute so that the volume fraction $Nv \ll 1$. Therefore the dynamic viscosity, μ, is assumed to be constant and equal in value to that of water. Changes in density, ρ, of an element of fluid due to cell diffusion, cell swimming and changes in pressure are assumed to be small and therefore the fluid is taken to be incompressible (the Boussinesq approximation). Hence

$$\boldsymbol{\nabla}\cdot\boldsymbol{U} = 0, \tag{1.1}$$

where $\boldsymbol{U}$ is the fluid velocity. Neglecting all effects of the cells except their negative buoyancy, the momentum equation is

$$\rho_w\left(\frac{\partial \boldsymbol{U}}{\partial T} + (\boldsymbol{U}\cdot\boldsymbol{\nabla})\,\boldsymbol{U}\right) = -\boldsymbol{\nabla}P_e + (\rho_c - \rho_w)vN\boldsymbol{g} + \mu\,\Delta\boldsymbol{U}, \tag{1.2}$$

where $P_e(\boldsymbol{X}, T)$ is the excess pressure above the hydrostatic pressure, $\boldsymbol{g}$ is the acceleration due to gravity and Δ is the Laplacian operator. These equations are the Navier–Stokes equations.

The cell and oxygen conservation equations are based on the Keller–Segel (1971*a*, *b*) equations, which have been successfully applied to a number of experimental situations. To account for the bulk fluid motion initiated when a convective instability forms, cell and oxygen advection terms, $N\boldsymbol{U}$ and $C\boldsymbol{U}$ respectively, are included in the conservation equations which are given by

$$\frac{\partial N}{\partial T} = -\boldsymbol{\nabla}\cdot[N(\boldsymbol{U}+\boldsymbol{V}) - \boldsymbol{D}\cdot\boldsymbol{\nabla}N], \tag{1.3}$$

and

$$\frac{\partial C}{\partial T} = -\boldsymbol{\nabla}\cdot(C\boldsymbol{U} - D_c\boldsymbol{\nabla}C) - KN, \tag{1.4}$$

where $\boldsymbol{V}$ is the average cell swimming velocity; $\boldsymbol{D}$ is the cell diffusivity tensor, consequent upon random cell swimming and therefore, like $\boldsymbol{V}$, dependent on C ($\boldsymbol{D}$ is taken to be isotropic with magnitude D_N); K is the rate at which an individual cell consumes oxygen; and D_c is the oxygen diffusivity. Two effects have been neglected in equation (1.3):

(i) gravitational sedimentation of cells, because the sedimentation speed of a 2 μm particle with $\Delta\rho/\rho = 0.1$ ($\sim 0.2\ \mu\text{m s}^{-1}$) is very much smaller than a typical cell swimming speed of 20 $\mu\text{m s}^{-1}$ (this will be inaccurate when the cells have become inactive, but is still unlikely to have much effect if the timescale for instability is sufficiently rapid);

(ii) the influence of rotation or straining in the ambient flow on the orientation and hence swimming direction of a cell. The latter process (rheotaxis or gyrotaxis) has been carefully analysed in the context of algal suspensions (Pedley & Kessler 1990) but it is not clear how to take it into account in the bacterial case, since the oxygen distribution is also influenced by fluid rotation.

In HPK we took the quantities arising in (1.3) and (1.4) to have the form

$$V = aV_{s0}\, W(\theta)\, \hat{\boldsymbol{e}}(|\nabla\theta| - \epsilon_0)\, H(|\nabla\theta| - \epsilon_0), \tag{1.5}$$

$$D_N = D_{N0}\, W^2(\theta), \tag{1.6}$$

$$K = K_0\, W(\theta), \tag{1.7}$$

$$D_c = \text{constant}, \tag{1.8}$$

where θ is a dimensionless measure of C:

$$\theta = \frac{C - C_{min}}{C_0 - C_{min}}, \tag{1.9}$$

and $W(\theta)$ is a saturating function with the characteristics $W(\theta) \to 1$ as $C \to \infty$ and $W(\theta) = 0$ when $C \leqslant C_{min}$. This function is introduced to represent the fact that the cells become inactive when the oxygen concentration falls below a small threshold value, C_{min}. The quantities a, V_{s0}, D_{N0}, K_0, ϵ_0 are dimensional constants, $\hat{\boldsymbol{e}}$ is a unit vector parallel to the oxygen concentration gradient $\nabla\theta$, and H is the Heaviside step function. A small cut-off oxygen concentration gradient, ϵ_0, was included in the expression for V since it was thought to be unlikely that the cells could distinguish extremely small oxygen concentration gradients. Further discussion regarding these choices can be found in HPK. For the purposes of this paper we restrict attention to the case in which $W(\theta) \equiv H(\theta)$, the step function. It is shown in HPK that the steady-state cell and oxygen concentration distributions are qualitatively consistent with experimental observations for this choice. In addition we assume that $\epsilon_0 = 0$, as non-zero values for the cut-off gradient were shown to have no qualitative effect on the steady-state cell and oxygen concentration distributions. These simplifications enabled HPK to find analytical steady-state solutions which considerably simplify the linear instability analysis.

The horizontal boundaries are at $Z = 0, h$, and the sidewalls are assumed to be sufficiently far away that the chamber effectively has infinite width. The boundary conditions on the oxygen concentration, C, are that it takes the given value C_0 at any interface with the air, and that there is zero flux at all other boundaries. The boundary condition on the cell concentration, N, will be taken to be the obvious one of zero flux, balancing chemotaxis and cell diffusion, at all boundaries of the suspension. Thus if $\boldsymbol{k}$ is a unit vector directed vertically upwards with respect to the chamber then

$$\theta = 1 \quad \text{at} \quad Z = 0, \tag{1.10}$$

$$\nabla\theta \cdot \boldsymbol{k} = 0 \quad \text{at} \quad Z = h, \tag{1.11}$$

$$[N(\boldsymbol{U} + V) - \boldsymbol{D} \cdot \nabla N] \cdot \boldsymbol{k} = 0 \quad \text{at} \quad Z = 0, h. \tag{1.12}$$

The initial, well-stirred condition, at $T = 0$, is that the oxygen and cell concentrations are uniform:

$$\theta(Z, 0) = 1, \quad N(Z, 0) = N_0. \tag{1.13}$$

In addition, we assume that the timescale for which biological growth and decay are significant is much greater than that required for pattern formation, so that the total number of cells is conserved. Hence, for all T,

$$\int_0^h N(Z,T)\,\mathrm{d}Z = N_0 h. \tag{1.14}$$

There are also conditions on the fluid velocity, U, at the boundaries. As the top of the chamber is exposed to the atmosphere, it is assumed to be free of tangential stress; this implies

$$\frac{\partial^2(\boldsymbol{U}\cdot\boldsymbol{k})}{\partial Z^2} = 0 \quad \text{at} \quad Z = 0 \tag{1.15}$$

(Chandrasekhar 1961). At the bottom of the chamber there is a rigid boundary, at which a no-slip condition is imposed, so that

$$\boldsymbol{U}\times\boldsymbol{k} = 0 \quad \text{at} \quad Z = h. \tag{1.16}$$

The vertical component of $\boldsymbol{U}$ is also zero at the boundaries of the chamber, hence

$$\boldsymbol{U}\cdot\boldsymbol{k} = 0 \quad \text{at} \quad Z = 0, h. \tag{1.17}$$

Equation (1.9) gives the dimensionless form, θ, of the oxygen concentration. We now introduce dimensionless forms of the other variables, as follows:

$$n = \frac{N}{N_0}, \quad z = \frac{Z}{h}, \quad t = \left(\frac{D_{N0}}{h^2}\right)T, \quad \boldsymbol{u} = \left(\frac{h}{D_{N0}}\right)\boldsymbol{U}, \quad p_e = \left(\frac{h^2}{\mu D_{N0}}\right)P_e. \tag{1.18}$$

In dimensionless form, the Navier–Stokes equation is

$$Sc^{-1}\left(\frac{\partial \boldsymbol{u}}{\partial t} + (\boldsymbol{u}\cdot\boldsymbol{\nabla})\boldsymbol{u}\right) = -\boldsymbol{\nabla}p_e - \Gamma n\boldsymbol{k} + \Delta\boldsymbol{u}, \tag{1.19}$$

where $Sc = \nu/D_{N0}$ is the Schmidt number, $\nu = \mu/\rho_w$ being the kinematic viscosity of the fluid, and the dimensionless number analogous to the Rayleigh number in thermal convection problems is

$$\Gamma = \frac{(\rho_c - \rho_w)\nu N_0 g}{\rho_w \nu D_{N0}} h^3. \tag{1.20}$$

This definition of Rayleigh number is different in two respects from that defined by Hill, Pedley & Kessler (1989) for suspensions of gyrotactic micro-organisms. First, the latter contains a measure of the surface cell concentrations N_s rather than initial concentration N_0, and secondly it includes the ratio of the chamber depth h to the scale height $L(= D_N/V_c$, where V_c is the cell swimming speed) of the undisturbed cell distribution. In our case we have no prior estimates of N_s or L, and Γ arises naturally. However, it may turn out not to be the most appropriate measure of instability; this point is further discussed in §5, with the aid of the numerical results to the full linear instability problem.

In dimensionless form the incompressibility condition is

$$\boldsymbol{\nabla}\cdot\boldsymbol{u} = 0, \tag{1.21}$$

and the cell and oxygen conservation equations are respectively given by

$$\frac{\partial n}{\partial t} = \boldsymbol{\nabla}\cdot(H(\theta)\boldsymbol{\nabla}n - \boldsymbol{u}n - H(\theta)\gamma n\boldsymbol{\nabla}\theta) \tag{1.22}$$

Initial cell concentration	$N_0 \approx 10^9$ cm^{-3}
Initial oxygen concentration	$C_0 \approx 1.5 \times 10^{17}$ molecules cm^{-3}
Max. cell diffusivity	$D_{N0} \approx 1.3 \times 10^{-6}$ cm^2 s^{-1}
Max. cell swimming speed	$V_{s0} \approx 2 \times 10^{-3}$ cm s^{-1}
Oxygen diffusivity	$D_c \approx 2.12 \times 10^{-5}$ cm^2 s^{-1}
Chemotaxis constant	$a \approx$ min (0.1h, 0.05 cm)
Max. oxygen consumption rate	$K_0 \approx 10^6$ molecules cell^{-1} s^{-1}
Cell density ratio	$(\rho_c - \rho_w)/\rho_w \approx 0.1$
Dynamic viscosity	$\mu \approx 10^{-2}$ g cm^{-1} s^{-1}
Cell volume	$v \approx 10^{-12}$ cm^3
Density of water	$\rho_w \approx 1.0$ g cm^{-3}
Kinematic viscosity	$\nu \approx 10^{-2}$ cm^2 s^{-1}

TABLE 1. Estimates of typical dimensional parameters for a suspension of *Bacillus subtilis*.

Diffusion parameter	$\delta \approx 16$
Depth parameter	$\beta \approx 7h^2$
Upswimming parameter	$\gamma \approx \begin{cases} 77 & \text{(deep chamber)} \\ 15h & \text{(shallow chamber)} \end{cases}$
Schmidt number	$Sc \approx 7700$
'Rayleigh number'	$\Gamma \approx 10^3 h^3$

TABLE 2. Estimates of the dimensionless parameters (h, where it appears, is measured in mm).

and
$$\frac{\partial \theta}{\partial t} = \nabla \cdot (\delta \nabla \theta - \boldsymbol{u}\theta) - H(\theta)\,\delta\beta\, n, \tag{1.23}$$

where the dimensionless constants are

$$\delta = \frac{D_c}{D_{N0}}, \quad \gamma = \frac{aV_{s0}}{D_{N0}}, \quad \beta = \frac{K_0 N_0 h^2}{D_c \Delta C}, \tag{1.24}$$

with $\Delta C = C_0 - C_{min}$. We can regard β as a depth parameter (it is a ratio of oxygen consumption rate to oxygen diffusion rate) and γ as a measure of the strength of the oxytactic swimming relative to the random, diffusive swimming. (Note that the quantity β was called β^2 by HPK.) The dimensionless boundary conditions are

$$\theta(0, t) = 1, \tag{1.25}$$

$$\nabla\theta \cdot \boldsymbol{k} = 0 \quad \text{at} \quad z = 1, \tag{1.26}$$

$$H(\theta)\frac{\partial n}{\partial z} + \gamma H(\theta) n \frac{\partial \theta}{\partial z} = 0 \quad \text{at} \quad z = 0, 1, \tag{1.27}$$

$$\frac{\partial^2 (\boldsymbol{u} \cdot \boldsymbol{k})}{\partial z^2} = 0 \quad \text{at} \quad z = 0, \tag{1.28}$$

$$\boldsymbol{u} \times \boldsymbol{k} = \boldsymbol{0} \quad \text{at} \quad z = 1, \tag{1.29}$$

$$\boldsymbol{u} \cdot \boldsymbol{k} = 0 \quad \text{at} \quad z = 0, 1. \tag{1.30}$$

Values of the physical quantities involved in the above model were estimated on the basis of Kessler's experiments, as reported by Kessler (1989) and Kessler *et al.* (1994, 1995), and were discussed by HPK; they are reproduced in table 1. Table 2 gives estimates for the dimensionless parameters γ, β, δ, Sc and Γ.

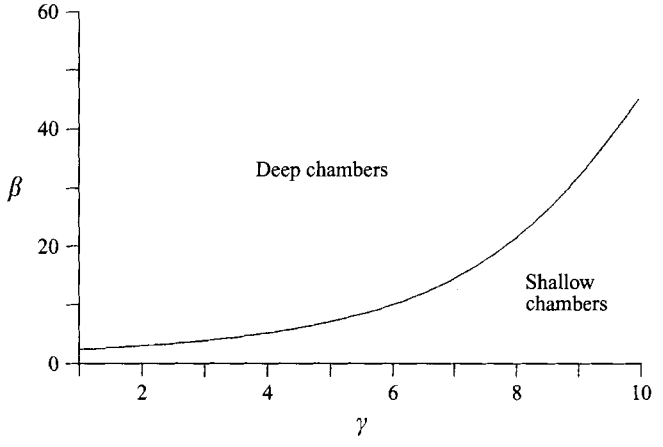

FIGURE 1. The curve in the (γ, β)-plane that separates 'deep' and 'shallow' chamber behaviours based on the asymptotic steady-state solution (see inequality (1.41)).

1.3. *Steady-state solutions*

The analytical steady-state distributions are derived in HPK and we state here only the results relevant to this analysis. These are divided into two categories according to whether or not the oxygen concentration reaches its minimum value in some region of the chamber. In 'shallow' chambers it is assumed that $\theta > 0$ and $|\nabla\theta| > 0$ for $0 \leqslant z < 1$; the steady-state solution is then given by

$$\theta(z) = 1 - \frac{2}{\gamma} \ln\left[\frac{\cos\{\frac{1}{2}A_1(1-z)\}}{\cos(\frac{1}{2}A_1)}\right] \tag{1.31}$$

and

$$n(z) = \frac{A_1^2}{2\gamma\beta} \sec^2\{\tfrac{1}{2}A_1(1-z)\}, \tag{1.32}$$

where the constant A_1 is determined from the transcendental equation:

$$\tan(\tfrac{1}{2}A_1) = \gamma\beta/A_1. \tag{1.33}$$

Note that the steady-state cell distribution depends only on the product $\gamma\beta$, though its evolution depends on γ and β separately (HPK).

In 'deep' chambers, as seen experimentally, an inactive zone of cells forms below a critical distance, $z = z_c$ (say), where $\theta = |\nabla\theta| = 0$ for $z_c \leqslant z \leqslant 1$. For $0 \leqslant z \leqslant z_c$ the steady-state solutions are given by

$$\theta(z) = \frac{2}{\gamma} \ln\{\sec(\tfrac{1}{2}A_2(z_c - z))\} \tag{1.34}$$

and

$$n(z) = \frac{A_2^2}{2\gamma\beta} \sec^2\{\tfrac{1}{2}A_2(z_c - z)\}, \tag{1.35}$$

with the condition

$$\tan(\tfrac{1}{2}A_2 z_c) = \gamma\beta\alpha_c/A_2, \tag{1.36}$$

where

$$A_2 = \alpha_c \gamma\beta/\phi, \tag{1.37}$$

$$z_c = \frac{2\phi}{\gamma\beta\alpha_c} \tan^{-1}(\phi), \tag{1.38}$$

$$\phi^2 = e^{\gamma} - 1, \tag{1.39}$$

and

$$\int_0^{z_c} n\,dz = \alpha_c. \tag{1.40}$$

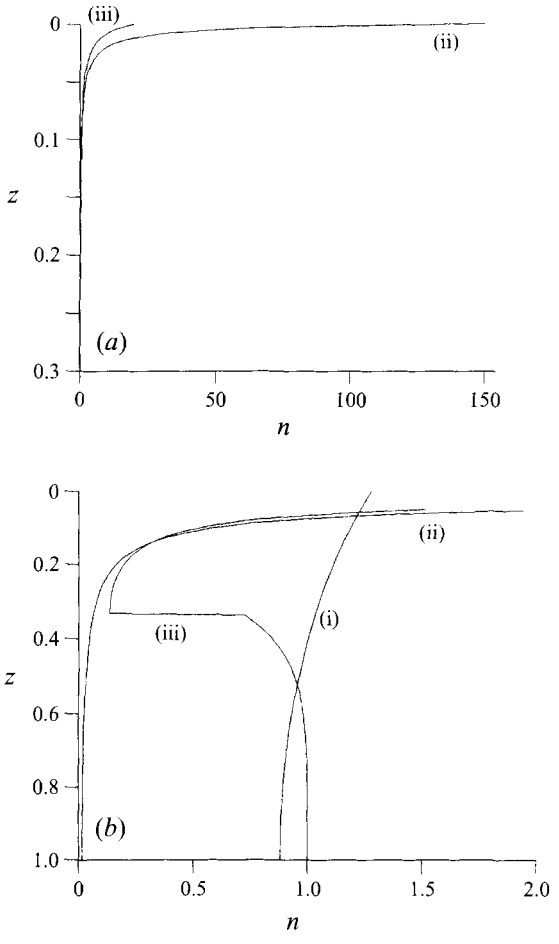

FIGURE 2. (*a*) Typical cell concentration profiles in the boundary layer region for shallow (curve ii: $\gamma\beta = 300$) and deep (curve iii: $\gamma = 5$, $\beta = 60$, $\delta = 1$) chamber examples ($\gamma\beta \gg 1$). (*b*) The cell concentration profiles in the main body of the chamber for the examples shown in (*a*), together with a typical concentration profile for a shallow-chamber example where no cell boundary layer forms ($\gamma\beta = 0.8$; curve i).

The fact that the cell diffusivity and cell swimming velocity are zero for $z > z_c$ means that an analytical solution for the cell concentration in $z > z_c$ cannot be obtained. In that zone n is not identically equal to 1 because, at first, there is an oxygen gradient and the cells continue to swim up it until θ falls to zero. Consequently, the value of $\alpha_c (0 < \alpha_c < 1)$ cannot be derived from the steady-state analysis and must instead be obtained from the numerical solution of the full initial value problem (see HPK). For this reason the deep-chamber steady-state cell distribution may depend separately on γ and β, as well as δ.

It can be shown that values of γ and β that satisfy the inequality

$$\gamma\beta \leqslant 2\phi \tan^{-1}\phi \tag{1.41}$$

correspond to shallow chambers; all other values correspond to deep chambers. To aid later explanations, a plot of the curve $\beta = (2/\gamma)\phi \tan^{-1}\phi$, henceforth referred to as the transition line, is shown in figure 1. In figure 2 are shown typical steady-state cell concentration distributions for both shallow and deep chambers. Note that in each

case (for $\gamma\beta \gg 1$) there is a 'boundary layer' of high cell concentration and concentration gradient near the upper surface of the chamber. Only for small depth (small $\gamma\beta$) does this not occur.

2. Formulation of the linear instability problem

The instability analysis involves linearizing the governing equations for small perturbations from the steady state, solving the resulting equations for a perturbation with a single horizontal wavenumber k^*, and calculating the corresponding temporal growth rate σ. In general, the eigenvalue σ is a complex number $\sigma_r + i\sigma_i$. If $\sigma_r > 0$ for any wavenumber k^* then the steady state is unstable. The values of σ_r and σ_i will depend on the dimensionless parameters of the system: β, γ, δ, Sc, Γ. In general, the system is stable ($\sigma_r < 0$ for all k^*) if Γ is less than a critical value Γ_c that depends on the other parameters, but unstable for $\Gamma > \Gamma_c$. We wish to compute Γ_c for a range of values of the other parameters.

It is also of interest to calculate σ_i for the marginal states in which $\sigma_r = 0$. If $\sigma_i = 0$, the corresponding instability is stationary; if $\sigma_i \neq 0$ it is oscillatory. In some problems it is straightforward to show analytically that the instability must be stationary; see Pedley, Hill & Kessler (1988) for example. However, attempts at such analysis in our case have been unsuccessful, even for a shallow chamber. In view of the above, all the theory will be directed towards investigating conditions for marginal stability by setting $\sigma_r = 0$ at the start, and treating Γ and σ_i as the eigenvalues to be found.

It is necessary to treat the shallow- and deep-chamber problems separately because the constraint $\theta \geqslant 0$ must be imposed, so not all conceivable perturbations in the zone $z > z_c$, where $\theta = 0$ in the steady state, are permitted. The shallow-chamber problem is dealt with first.

2.1. *Shallow chamber*

Here, the perturbations to the steady state are given by

$$\boldsymbol{u}(\boldsymbol{x}, t) = \epsilon \boldsymbol{u}_1'(\boldsymbol{x}, t), \tag{2.1a}$$

$$n(\boldsymbol{x}, t) = n(z) + \epsilon n_1'(\boldsymbol{x}, t), \tag{2.1b}$$

$$\theta(\boldsymbol{x}, t) = \theta(z) + \epsilon \theta_1'(\boldsymbol{x}, t), \tag{2.1c}$$

$$p_e(\boldsymbol{x}, t) = p_e(z) + \epsilon p_e'(\boldsymbol{x}, t), \tag{2.1d}$$

where $0 \leqslant \epsilon \ll 1$. The components of $\boldsymbol{u}_1'$ are (u_1', v_1', w_1'). On substitution of (2.1 *a–d*) into the governing equations, and elimination of p_e', u_1' and v_1', these equations can be expressed in terms of w_1', n_1' and θ_1' only. These quantities are then decomposed into normal modes of the form,

$$[n_1', \theta_1', w_1'] = [N_1(z), C_1(z), W_1(z)] f(x, y) \mathrm{e}^{\sigma t},$$

where the horizontal planform function, f, satisfies

$$\Delta_h f = -k^2 f, \tag{2.2}$$

with

$$\Delta_h = \frac{\partial}{\partial x^2} + \frac{\partial}{\partial y^2},$$

and k is a constant dimensionless wavenumber, defined by

$$k = k^* h, \tag{2.3}$$

which corresponds to the dimensionless wavelength,

$$\lambda = 2\pi/k. \tag{2.4}$$

The perturbation equations become

$$\frac{\mathrm{d}^2 N_1}{\mathrm{d}z^2} - (\sigma + k^2) N_1 = \left(\gamma\beta n + \gamma \frac{\mathrm{d}^2\theta}{\mathrm{d}z^2}\right) N_1 + \gamma \frac{\mathrm{d}\theta}{\mathrm{d}z}\frac{\mathrm{d}N_1}{\mathrm{d}z} + \gamma \frac{\mathrm{d}n}{\mathrm{d}z}\frac{\mathrm{d}C_1}{\mathrm{d}z} + \left(\frac{\mathrm{d}n}{\mathrm{d}z} + \frac{\gamma}{\delta} n \frac{\mathrm{d}\theta}{\mathrm{d}z}\right) W_1 + \frac{\gamma\sigma n}{\delta} C_1, \tag{2.5a}$$

$$\frac{\mathrm{d}^2 C_1}{\mathrm{d}z^2} - \left(\frac{\sigma}{\delta} + k^2\right) C_1 = \beta N_1 + \left(\frac{1}{\delta}\right)\frac{\mathrm{d}\theta}{\mathrm{d}z} W_1, \tag{2.5b}$$

$$\left(\frac{\mathrm{d}^2}{\mathrm{d}z^2} - (k^2 + \sigma Sc^{-1})\right)\left(\frac{\mathrm{d}^2}{\mathrm{d}z^2} - k^2\right) W_1 = k^2 N_1 \Gamma, \tag{2.5c}$$

subject to the boundary conditions

$$C_1 = 0 \quad \text{at} \quad z = 0, \tag{2.6a}$$

$$W_1 = 0 \quad \text{at} \quad z = 0, 1, \tag{2.6b}$$

$$\frac{\mathrm{d}N_1}{\mathrm{d}z} - \gamma\left(n(0)\frac{\mathrm{d}C_1}{\mathrm{d}z} + \left.\frac{\mathrm{d}\theta}{\mathrm{d}z}\right|_{z=0} N_1\right) = 0 \quad \text{at} \quad z = 0, \tag{2.6c}$$

$$\frac{\mathrm{d}N_1}{\mathrm{d}z} = \frac{\mathrm{d}C_1}{\mathrm{d}z} = 0 \quad \text{at} \quad z = 1, \tag{2.6d}$$

$$\frac{\mathrm{d}^2 W_1}{\mathrm{d}z^2} = 0 \quad \text{at} \quad z = 0, \tag{2.6e}$$

and

$$\frac{\mathrm{d}W_1}{\mathrm{d}z} = 0 \quad \text{at} \quad z = 1. \tag{2.6f}$$

It should be noted that this shallow-chamber instability problem depends on γ and β only through the product $\gamma\beta$. This follows from (1.31)–(1.33) where we see that $n(z)$ depends only on $\gamma\beta$ (already noted) and $\mathrm{d}\theta/\mathrm{d}z$ can be written as the product of β and a function of z and $\gamma\beta$. If, in (2.5)–(2.6), C_1 is replaced by $\beta\bar{C}_1$, then the dependence on $\gamma\beta$ becomes clear.

The governing equations (2.5*a–c*) form an eighth-order system with coefficients that are functions of z; this system cannot, in general, be solved analytically. Only for very shallow chambers, where $\beta \ll 1$, has it been possible to find an analytical approximation to the solution (see §3.1).

2.2. *Deep chamber*

The deep-chamber stability problem is quite different from that of the shallow chamber because the steady state both may depend on γ and β separately and consists of an unstable region above a stable one (see figure 2*b*). At the onset of instability, the fluid motions initiated in the upper unstable layer are likely to penetrate into the lower, stable layer. The distance of penetration will depend on a variety of factors, but the position of the cut-off point, z_c, and the measure of the cell stratification in the upper and lower layers will be of primary importance.

Penetrative convection has been considered by a number of authors, for example Veronis (1963), mainly in a thermal convection context, and is usually defined by a

single set of equations valid over the entire domain of interest (though Stix 1970 and Zahn, Toomre & Latour 1982 considered multi-layer models). This however does not apply in the present case because of the cut-off for $\theta \leqslant 0$ of the cell diffusivity, cell swimming speed and oxygen consumption rate. In the lower region of inactive cells, we would expect θ to remain zero and the cell concentration to change solely as a result of advection with the fluid motion driven from above. The position of the interface between active and inactive cells will also be deformed by the motion, and may be expressed in the form

$$z = z_c + \epsilon\xi(x, t) = z_I. \tag{2.7}$$

Henceforth we will denote the region $0 \leqslant z < z_I$ as region 1, and $z_I < z \leqslant 1$ as region 2. Appropriate matching conditions must be imposed on n, θ and $\boldsymbol{u}$ at the interface. Note that, while the steady-state solution in the region $0 \leqslant z \leqslant z_c$ is known analytically (equations (1.34)–(1.36)), the steady-state values of $n(z)$ for $z > z_c$ are known only numerically, at discrete values of z.

The cell conservation equation in region 2 is given by

$$\frac{\partial n}{\partial t} = -\nabla\cdot(\boldsymbol{u}n) \tag{2.8}$$

(advection only). The oxygen concentration equation is not required in region 2 because $\theta \equiv 0$. The Navier–Stokes equation is still given by (1.19). The perturbations in region 2 are denoted by the suffix 2, e.g.

$$n(\boldsymbol{x}, t) = n(z) + \epsilon N_2(z) f(x, y)\, \mathrm{e}^{\sigma t}.$$

Proceeding as in the shallow-chamber case we obtain the following fourth-order system of linearized equations:

$$\left(\frac{\mathrm{d}^2}{\mathrm{d}z^2} - (k^2 + \sigma Sc^{-1})\right)\left(\frac{\mathrm{d}^2}{\mathrm{d}z^2} - k^2\right) W_2 = k^2 N_2 \Gamma, \tag{2.9a}$$

$$\sigma N_2 + \frac{\mathrm{d}n}{\mathrm{d}z} W_2 = 0. \tag{2.9b}$$

In the upper region, the governing equations have the same form as in the shallow-chamber case, equations (2.5). The surface boundary conditions in that case are also relevant for deep chambers. At the bottom of the chamber, all components of the fluid velocity are again zero, as is the cell flux. Thus the conditions on the perturbations at $z = 1$ are

$$W_2 = \frac{\mathrm{d}W_2}{\mathrm{d}z} = 0 \tag{2.10a}$$

and

$$\frac{\mathrm{d}N_2}{\mathrm{d}z} = 0 \quad \text{at} \quad z = 1 \tag{2.10b}$$

(2.10b is not independent, following from (2.9b) and (2.10a), unless $\sigma = 0$).

It remains to specify the matching conditions at the interface. Continuity of the oxygen concentration and oxygen flux implies that, at the interface,

$$\theta_1 = 0 \tag{2.11a}$$

and

$$\nabla\theta_1 \cdot \hat{\boldsymbol{z}} = 0, \tag{2.11b}$$

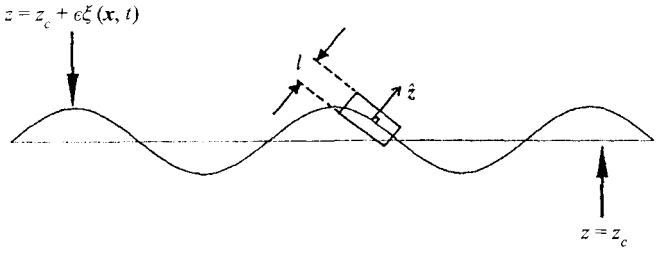

FIGURE 3. Perturbation of the interface between active and inactive cells due to advection by the fluid motion.

where $\hat{z}$ is a unit vector normal to the interface, with unit vertical component and an $O(\epsilon)$ horizontal component, and the suffix 1 refers to region 1. In Fourier mode representation we let

$$\xi(\boldsymbol{x}, t) = \chi f(x, y)\, \mathrm{e}^{\sigma t},$$

where χ is a constant, and the linearized forms of (2.11*a*, *b*) become

$$C_1 = 0 \tag{2.12a}$$

and

$$\frac{\mathrm{d}C_1}{\mathrm{d}z} = -\chi \left.\frac{\mathrm{d}^2\theta}{\mathrm{d}z^2}\right|_{z=z_{c-}} \tag{2.12b}$$

respectively. In fact condition (2.12*b*) is useful only for the determination of χ.

We also require a condition on N_1 at the interface. This is obtained by integrating the rate of change in cell concentration over a rectangle of height l and of unit area whose centre coincides with a point on the interface, as depicted in figure 3. As $l \to 0$, then

$$\int_{-l/2}^{l/2} \left(\frac{\partial n}{\partial t}\right) \mathrm{d}\hat{z} \to 0;$$

i.e. there can be no finite cell accumulation in a region of zero thickness. With $\partial n/\partial t$ given by (2.8) and (1.22), the above integral gives the condition

$$\{\hat{z}\cdot\nabla n - (\boldsymbol{u}n)\cdot\hat{z} - \gamma n \nabla\theta\cdot\hat{z}\}_{z\to z_{c-}} - (-\boldsymbol{u}n\cdot\hat{z})_{z\to z_{c+}} = 0. \tag{2.13}$$

Finally, continuity of the fluid velocity and its gradients across the interface implies

$$\boldsymbol{u}_1' = \boldsymbol{u}_2', \quad \frac{\partial^i \boldsymbol{u}_1'}{\partial z^i} = \frac{\partial^i \boldsymbol{u}_2'}{\partial z^i} \quad \text{for} \quad i = 1, 2, 3 \tag{2.14}$$

at $z = z_c + \xi$. Linearized and expressed in terms of a Fourier mode, conditions (2.13) and (2.14) become

$$\frac{\mathrm{d}N_1}{\mathrm{d}z} - \gamma n(z_{c-})\frac{\mathrm{d}C_1}{\mathrm{d}z} - W_1 n(z_{c-}) + W_2 n(z_{c+}) = 0 \tag{2.15}$$

and

$$W_1 = W_2, \quad \frac{\mathrm{d}^i W_1}{\mathrm{d}z^i} = \frac{\mathrm{d}^i W_2}{\mathrm{d}z^i} \quad \text{for} \quad i = 1, 2, 3 \tag{2.16}$$

respectively.

In all cases considered, we shall specify the *mode* of any solution in terms of the number of times $W(z)$ changes sign in the interval $0 \leqslant z \leqslant 1$: mode L corresponds to $L-1$ sign changes.

3. Shallow-chamber methods and results

In problems where there is only one physical mechanism for instability, the instability is normally stationary. (Oscillatory instability was predicted by Hill *et al.* 1989 for an algal suspension in which two independent instability mechanisms could be identified.) Thus, in shallow chambers we assume that the marginal state will be *stationary*. In the absence of a formal proof, this assumption was verified for all parameter values of interest by solving numerically the linear instability problem for the eigenvalues σ_i and Γ, given $\sigma_r = 0$. Note that N_1, C_1 and W_1 must be treated as complex functions. It was indeed found that $\sigma_i = 0$ (and $\Gamma > 0$) in all of the shallow-chamber cases tested. Furthermore, the analytical solution with $\gamma\beta \ll 1$ (§3.1) also gives $\sigma \in \mathbb{R}$.

3.1. *Analytical solutions for small depth*

In this section analytical solutions to equations (2.5*a–c*) are given for very small values of the depth parameter, $\gamma\beta$. It is first necessary to expand the steady-state solutions (1.31)–(1.33) in powers of $\gamma\beta$. The expansion for A_1 in equation (1.33) is found to be

$$A_1 = (2\gamma\beta)^{1/2}\left(1 - \frac{\gamma\beta}{12} + \frac{7\gamma^2\beta^2}{288} + O(\gamma^3\beta^3)\right), \tag{3.1}$$

and then (1.32) gives

$$n(z) = 1 + \tfrac{1}{2}\{(1-z)^2 - \tfrac{1}{3}\}\gamma\beta + \tfrac{1}{6}\{\tfrac{7}{24} - (1-z)^2 + (1-z)^4\}\gamma^2\beta^2 + O(\gamma^3\beta^3). \tag{3.2}$$

Similarly the oxygen concentration gradient in the steady state, which also appears in the governing equations, is given by

$$\frac{\mathrm{d}\theta}{\mathrm{d}z} = -\beta\{(1-z) + \tfrac{1}{6}\gamma\beta(1-z)[(1-z)^2 - 1]\} + O(\gamma^2\beta^3). \tag{3.3}$$

If it is assumed that N, C and W (dropping the suffix 1 for the remainder of this section) can each be expressed as a series in powers of $\gamma\beta$ then it is possible to obtain the leading-order term (and higher orders if desired) in each of the series. For simplicity we also consider small wavenumbers, where $k \sim (\gamma\beta)^{1/2}$, so that

$$\tilde{k}^2 = k^2/\gamma\beta \tag{3.4}$$

is of order one; this corresponds to keeping the dimensional wavenumber fixed as $h \to 0$. For a non-trivial solution, both the highest-order derivative and the right-hand side must be retained in equation (2.5*c*) at leading order. This equation will therefore reduce to

$$\left(\frac{\mathrm{d}^2}{\mathrm{d}z^2} - \sigma Sc^{-1}\right)\frac{\mathrm{d}^2 W}{\mathrm{d}z^2} = \gamma\beta\tilde{k}^2\Gamma N, \tag{3.5}$$

which means in physical terms, and leaving aside the time dependence σ, that the viscous force, $\mathrm{d}^4 W/\mathrm{d}z^4$, balances the buoyancy force on the right-hand side. Without loss of generality, we also specify that

$$N = 1 \quad \text{at} \quad z = 0, \tag{3.6}$$

and set $C = \beta\bar{C}$. There are then two possible leading-order balances in equations (2.5*a*) and (2.5*b*), which potentially lead to non-trivial solutions, as follows:

case (i)

$$\Gamma \sim O(1), \quad \sigma \sim O(\gamma\beta), \quad \frac{\mathrm{d}^2\bar{C}}{\mathrm{d}z^2} = N, \quad \frac{\mathrm{d}^2 N}{\mathrm{d}z^2} = 0.$$

case (ii)

$$\Gamma \sim O(\gamma^{-1}\beta^{-1}), \quad \sigma \sim O(\gamma\beta), \quad \frac{\mathrm{d}^2\bar{C}}{\mathrm{d}z^2} = N - \frac{1-z}{\delta}W, \quad \frac{\mathrm{d}^2 N}{\mathrm{d}z^2} = 0.$$

In case (i), the leading-order balance in the cell conservation equation is purely diffusive, and in the oxygen conservation equation there is a balance between diffusion and consumption of oxygen. In case (ii), the leading-order balance in the cell conservation equation is the same, but in the oxygen conservation equation, advection is important as well as the other terms. It turns out that case (i) leads to negative values of σ, i.e. stability, in all circumstances (see Hillesdon 1994), so we here give the analysis only for case (ii). During the analysis which follows, the function $N_0(z)$ is not to be confused with the initial cell concentration, N_0.

In this case we seek expansions of the form

$$N(z) = \sum_{i=0}^{\infty} N_i(z)(\gamma\beta)^i, \quad \bar{C}(z) = \sum_{i=0}^{\infty} \bar{C}_i(z)(\gamma\beta)^i, \quad W(z) = \sum_{i=0}^{\infty} W_i(z)(\gamma\beta)^i$$

and

$$\sigma(\tilde{k}) = \sum_{i=1}^{\infty} \sigma_i(\tilde{k})(\gamma\beta)^i, \quad \Gamma(\tilde{k}) = \sum_{i=-1}^{\infty} \Gamma_i(\tilde{k})(\gamma\beta)^i.$$

At leading order, the governing equations become

$$\frac{\mathrm{d}^4 W_0}{\mathrm{d}z^4} = \tilde{k}^2\Gamma_{-1}N_0, \quad \frac{\mathrm{d}^2\bar{C}_0}{\mathrm{d}z^2} = N_0 - \frac{\bar{z}}{\delta}W_0, \quad \frac{\mathrm{d}^2 N_0}{\mathrm{d}z^2} = 0,$$

subject to the boundary conditions

$$W_0 = 0 \quad \text{at} \quad z = 0,1, \quad \frac{\mathrm{d}W_0}{\mathrm{d}z} = 0 \quad \text{at} \quad z = 1, \quad \frac{\mathrm{d}^2 W_0}{\mathrm{d}z^2} = 0 \quad \text{at} \quad z = 0,$$

$$\bar{C}_0 = 0 \quad \text{at} \quad z = 0,$$

$$\frac{\mathrm{d}N_0}{\mathrm{d}z} = 0 \quad \text{at} \quad z = 0,1, \quad \frac{\mathrm{d}\bar{C}_0}{\mathrm{d}z} = 0 \quad \text{at} \quad z = 1,$$

and we arbitrarily set $N_0 = 1$ at $z = 0$. The corresponding solution is

$$N_0(z) = 1, \tag{3.7a}$$

$$\bar{C}_0(z) = \tfrac{1}{2}(\bar{z}^2 - 1) - (20\bar{z}^7 - 70\bar{z}^6 + 63\bar{z}^5 - 13)\frac{2}{8!\delta}\Gamma_{-1}\tilde{k}^2, \tag{3.7b}$$

$$W_0(z) = \tfrac{1}{48}\Gamma_{-1}\tilde{k}^2(2\bar{z}^4 - 5\bar{z}^3 + 3\bar{z}^2), \tag{3.7c}$$

where, for convenience, we have taken $\bar{z} = 1 - z$.

At the next order the governing equations are

$$\frac{\mathrm{d}^4 W_1}{\mathrm{d}z^4} = (2\tilde{k}^2 + \sigma_1 Sc^{-1})\frac{\mathrm{d}^2 W_0}{\mathrm{d}z^2} + \tilde{k}^2(\Gamma_{-1}N_1 + \Gamma_0 N_0),$$

$$\frac{\mathrm{d}^2 N_1}{\mathrm{d}z^2} = (\sigma_1 + \tilde{k}^2 + 1) + \frac{\mathrm{d}^2\bar{C}_0}{\mathrm{d}z^2} + (z-1)W_0,$$

$$\frac{\mathrm{d}^2\bar{C}_1}{\mathrm{d}z^2} = \left(\tilde{k}^2 + \frac{\sigma_1}{\delta}\right)\bar{C}_0 + N_1 - \frac{1}{\delta}\{(1-z)W_1 - \tfrac{1}{3}(1-z)(1-2z^2-2z)W_0\},$$

subject to the boundary conditions,

$$W_1 = 0, \quad \bar{C}_1 = 0, \quad \frac{\mathrm{d}^2 W_1}{\mathrm{d}z^2} = 0, \quad \frac{\mathrm{d}N_1}{\mathrm{d}z} + 1 - \frac{\mathrm{d}\bar{C}_0}{\mathrm{d}z} = 0 \quad \text{at} \quad z = 0,$$

$$W_1 = 0, \quad \frac{\mathrm{d}W_1}{\mathrm{d}z} = 0, \quad \frac{\mathrm{d}N_1}{\mathrm{d}z} = 0, \quad \frac{\mathrm{d}\bar{C}_1}{\mathrm{d}z} = 0 \quad \text{at} \quad z = 1.$$

The solution of the problem at this order gives the functions N_1, W_1 and $\bar{C}_1$, and in addition determines σ_1 to be

$$\sigma_1 = \tilde{k}^2\left(\frac{1}{576}\Gamma_{-1} - 1\right). \tag{3.8}$$

The fact that W_0 has no internal zero shows that the vertical structure is that of a single bioconvection cell, so the disturbance is of mode 1. We see from (3.8) that the system is unstable to small-wavenumber disturbances if $\Gamma_{-1} > 576$. These results demonstrate that the instability is non-oscillatory. Marginal stability ($\sigma = 0$) occurs when

$$\Gamma(\tilde{k}) = \frac{576}{\gamma\beta} + O(1). \tag{3.9}$$

At the next order, we find that the second term in the series for σ is given by

$$\begin{aligned}\sigma_2 = {} & \tfrac{1}{3}\{(1+\tilde{k}^2)(2\sigma_1 + \tilde{k}^2) + \sigma_1^2\} + \frac{50}{3.8!}\left(1+\frac{1}{\delta}\right)\Gamma_{-1}\tilde{k}^2 + \frac{5}{4.6!}\Gamma_0\tilde{k}^2 \\ & + \frac{1}{5.8!}\Gamma_{-1}\tilde{k}^2\left(236\tilde{k}^2 + \sigma_1(212 + 17/Sc) + 324 + \frac{100}{\delta}(1+\sigma_1)\right) \\ & + \frac{1}{2.13!}\left(1+\frac{1}{\delta}\right)\Gamma_{-1}^2\tilde{k}^4\left(\frac{5.19.581}{\delta} - 180.307\left(1+\frac{1}{\delta}\right) + \frac{413.33.13}{4}\right).\end{aligned} \tag{3.10}$$

The correction Γ_0 to the value (3.9) of $\Gamma(\tilde{k})$ for marginal stability can now be found in terms of Γ_{-1} and $\tilde{k}^2$ using (3.10). These analytical results can be used to check the values of $\Gamma(k)$ found by numerical solution for $\sigma_r = 0$.

3.2. *Numerical results and discussion*

For fixed values of β, γ, δ and k the eighth-order system of equations (2.5*a–c*) is augmented by the further equation

$$\frac{\mathrm{d}\Gamma}{\mathrm{d}z} = 0$$

(and $\mathrm{d}\sigma_i/\mathrm{d}z = 0$ in cases where $\sigma_i = 0$ is not assumed), and the values of Γ (and σ_i) are sought for which the system has a non-trivial neutral solution with $\sigma_r = 0$. The ordinary differential equations were discretized using either a second-order centred Euler or box scheme (Keller 1974) or a fourth-order Runge–Kutta scheme (Cash & Moore 1980). The discretization meshes (clustered near the upper surface in cases for which the basic state has a thin cell boundary layer) were chosen so that the two methods gave the same results. Accuracy was enhanced using Richardson extrapolation; the difference equations were solved by Newton's method. Initial guesses for the functions $W_1(z)$, $N_1(z)$, $C_1(z)$, and the constants Γ (and σ_i) were obtained from analytical solutions, if available, or from previous computations at neighbouring

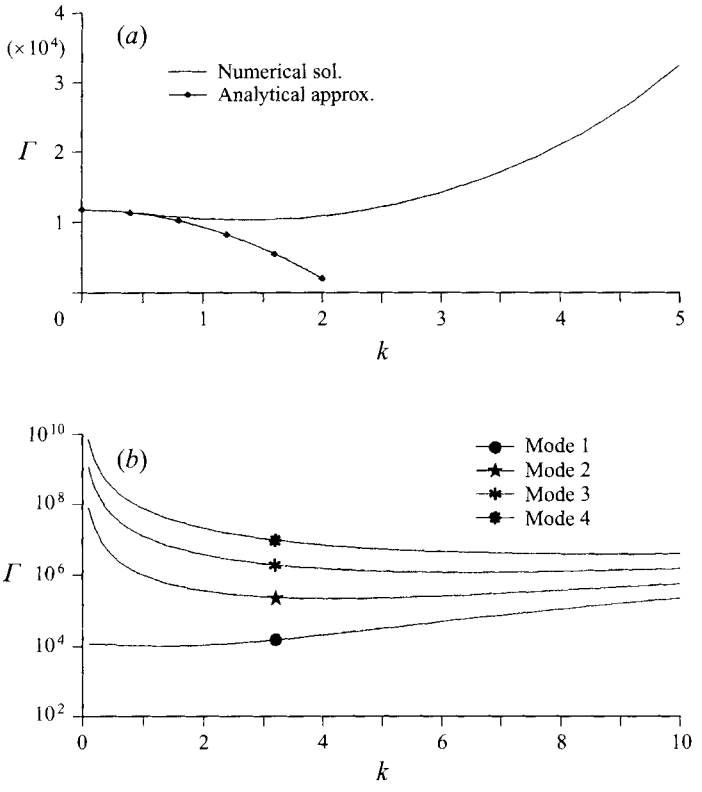

FIGURE 4. Example with $\delta = 1$, $\gamma\beta = 0.05$. (*a*) Comparison between numerical and analytical solutions for $\Gamma(k)$. (*b*) The $\Gamma(k)$ curves for the mode 1–4 solutions.

parameter values, or roughly sinusoidal variations of the functions were chosen. Note that different initial guesses for Γ can cause convergence to different modes of solution. Full details of the numerical method can be found in Hillesdon (1994).

The objective is to plot the neutral curve $\Gamma(k)$, and compute its minimum, giving critical values of Rayleigh number and wavenumber, Γ_c and k_c, for any values of the governing parameters we might choose. These are δ (oxygen versus cell diffusion), β (oxygen consumption versus oxygen diffusion) and γ (directed versus random cell swimming), as defined in (1.24); in shallow chambers the last two can be combined into the product $\gamma\beta$. It may be helpful to think of β (or $\gamma\beta$) as a depth parameter. Since there is great uncertainty about the value of the parameters, it is important to consider a range of values rather than limit ourselves to particular estimates such as those given in table 2.

To illustrate the comparison between the analytical and the numerical solution for $\gamma\beta \ll 1$, we plot in figure 4(*a*) the neutral curve $\Gamma(k)$ for the case $\gamma\beta = 0.05$, $\delta = 1$ (mode 1 solution). It can be seen that the two curves agree extremely well for $k \leqslant 0.06$. As $k \to 0$, the numerical results give $\Gamma \to 1.17 \times 10^4$, while the analytical approximation is $\Gamma \to 576/\gamma\beta = 1.15 \times 10^4$; the agreement improves as $\gamma\beta$ is further reduced. The critical values of the Rayleigh number and wavenumber are $\Gamma_c = 1.02 \times 10^4$ and $k_c = 1.37$ (as usual, if the latter has error ϵ, the former has error only $O(\epsilon^2)$). The critical wavenumber k_c gives an estimate for the dimensionless wavelength $\lambda_c = 2\pi/k_c$ of the first patterns to be observed in an experiment in which Γ is slowly raised above Γ_c. However, the most unstable disturbance for $\Gamma > \Gamma_c$ in general has a different

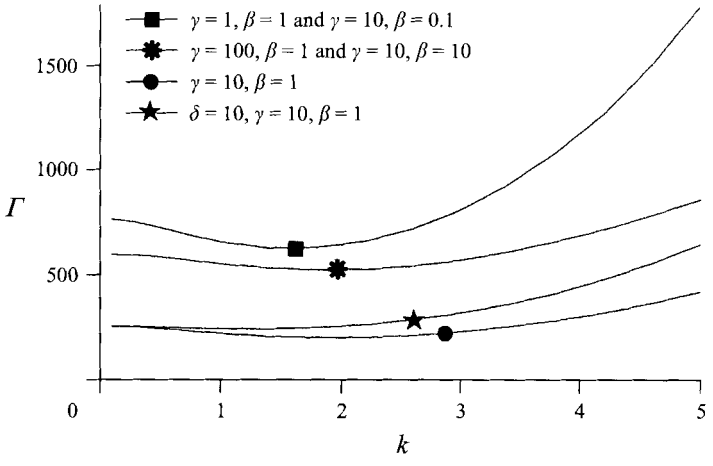

FIGURE 5. Neutral curves $\Gamma(k)$ calculated for a variety of shallow-chamber examples; $\delta = 1$ unless otherwise stated.

δ	$\gamma\beta$	Γ_c	k_c
1	0.05	1.02×10^4	1.37
1	1	625	1.58
1	10	200	1.90
1	50	328	1.94
1	100	522	1.91
10	10	241	1.29

TABLE 3. Values of Γ_c, k_c for various shallow-chamber examples.

wavelength; computations of σ_r for a given $\Gamma > \Gamma_c$ give a maximum when $k = k_m$ which is somewhat greater than k_c.

To investigate other modes of disturbance, the problem was solved with a variety of initial estimates for the eigenvalue $\Gamma(k)$ and the solution converged to different eigenfunctions. Figure 4(*b*) shows the neutral curves for the mode 1, 2, 3 and 4 solutions. Clearly the mode 1 solution is the most unstable; this is true for all shallow-chamber examples considered.

We now present the results for a variety of shallow-chamber examples, covering the whole range of steady-state density profiles, from nearly uniform ($\gamma\beta = 0.05$) to densely packed at the top ($\gamma\beta = 300$; figure 2, curves ii). It should be recalled that the steady-state profiles (for a shallow chamber) are independent of δ, varying only with $\gamma\beta$. Six sets of results for Γ_c and k_c are given in table 3, while the neutral curves $\Gamma(k)$ are plotted for four of these cases in figure 5.

Two features of the results are of interest. First we see that the neutral curves for different values of δ diverge as the wavenumber increases, despite the fact that the steady states are the same. The value of Γ, for a given k, is larger for $\delta = 10$ than for $\delta = 1$, i.e. an increase in δ is apparently stabilizing. However, interpretation of this result is not straightforward. The increase in the value of δ can be viewed either as an increase in D_c with D_{N0} fixed, or as a decrease in D_{N0} with D_c fixed. In the former case, a tenfold increase in D_c means that the value of $aV_{s0}K_0N_0h^2/D_{N0}\Delta C$ would also have to increase tenfold to keep $\gamma\beta$ fixed (see (1.24)). If this increase is attributed to an increase in the depth, h, then since $\Gamma \propto h^3$ the value of Γ will be greater by a factor of

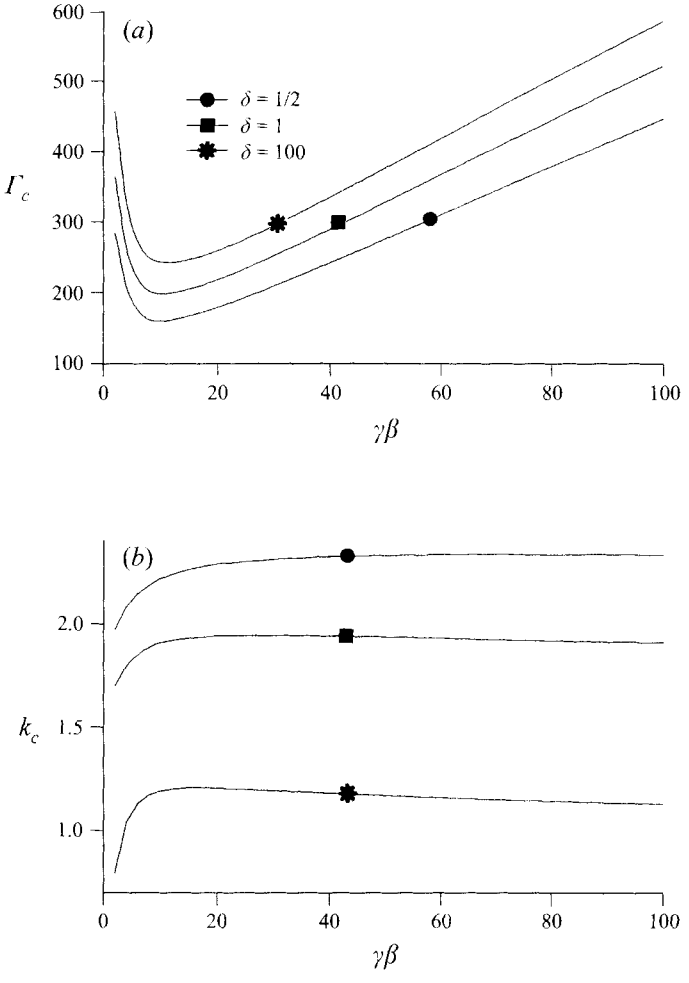

FIGURE 6. (*a*) Computed values of Γ_c, and (*b*) corresponding values of k_c, as the value of $\gamma\beta$ is varied for given values of δ. In (*a*), each curve has its minimum at $\gamma\beta \approx 9.9$.

$10^{3/2}$, more than the computed increase in Γ_c. In that sense the increase in δ can be thought of as destabilizing. The opposite conclusion is reached if the increase in δ results from a decrease in D_{N0}.

The second and probably more important comparison is between cases with different steady-state cell and oxygen distributions (i.e. different $\gamma\beta$) and, for convenience, the same value of $\delta (= 1)$. We would expect that the steeper free-surface density gradients, for larger values of $\gamma\beta$, should be more unstable. However, we see from table 3 that Γ_c at first falls as $\gamma\beta$ is increased, as expected, but then rises again; also k_c has a maximum value, though apparently not at the same value of $\gamma\beta$ as the minimum in Γ_c. To examine this behaviour more fully, the values of Γ_c and k_c are plotted against $\gamma\beta$ for different values of δ in figures 6(*a*) and 6(*b*). For each value of δ, the overall minimum value of Γ_c occurs when $\gamma\beta \approx 9.9$.

These findings suggest that Γ may not be the most appropriate measure of the ratio between the buoyancy forces that drive the bioconvection and the viscous forces that inhibit it. In the additional light of the deep-chamber numerical results (see §4) we show in §5 that more intuitively reasonable behaviour can be obtained by a different

choice of scaling for the Rayleigh number when $\gamma\beta \gg 1$, although Γ, as defined in (1.20), arose naturally from the non-dimensionalization of the problem.

4. Deep-chamber analysis and numerical results

4.1. *Characteristics of deep-chamber instability*

The following argument indicates that in deep chambers the marginal state must be oscillatory ($\sigma_i \neq 0$) whenever the corresponding wavenumber is also non-zero. The argument is based on the fact that the steady-state cell concentration gradient, $\mathrm{d}n/\mathrm{d}z$, is non-zero for $z > z_c$. If we assume a stationary marginal state, so that $\sigma_i = 0$, then equation (2.9*b*) for $z_c < z \leqslant 1$ gives $W_2 = 0$, which suggests that there is no penetrative convection, and then (2.9*a*) gives $N_2 = 0$ as long as $k^2 \neq 0$. Moreover, continuity of the velocity and stress at the interface then requires that W_1 and its first three derivatives are continuous, i.e. zero, at the interface. Together with (2.12*a*), (2.15) (which reduces to $\mathrm{d}N_1/\mathrm{d}z = \gamma n(z_{c-})\,\mathrm{d}C_1/\mathrm{d}z$), and the four conditions at $z = 0$ from (2.6*a–c*, *e*), this means that the eighth-order homogeneous system of differential equations (2.5) in the unstable region, $0 \leqslant z < z_c$, must satisfy 10 independent boundary conditions and there is only one adjustable constant, Γ. Hence the solution is identically zero. For a non-trivial solution, therefore, we must have $\sigma_i \neq 0$ or $k^2 = 0$.

Oscillatory instabilities generally occur when there are two competing physical mechanisms at work, one stabilizing and one destabilizing, as for example in double-diffusive convection. Double-diffusive instabilities do not occur in our system, despite the fact that there are two diffusing species (oxygen and cells), because only one of them contributes to the fluid density. In our case the destabilizing mechanism comes from the unstable density stratification in the upper region while the stabilizing one must arise from the stable density stratification in the lower region. A small disturbance of finite wavelength applied to the lower region alone would lead to oscillatory internal gravity waves, with a frequency determined by a combination of the density jump across $z = z_c$ and the density gradient below it.

4.2. *Numerical considerations*

Here the chamber has to be split into two zones and the solutions matched at the interface $z = z_c$. The functions $W_j(z)$, $C_j(z)$ and $N_j(z)$ ($j = 1, 2$) have to be split into real and imaginary parts, and the resulting systems of equations rewritten as sets of first-order equations. In the upper zone the system has order 16; in the lower zone it has order 8. A complication in the lower zone is that the basic cell concentration gradient $\mathrm{d}n/\mathrm{d}z$ is known only numerically, at particular values of z, from the initial value solution of HPK. Therefore its values at the chosen mesh points had to be interpolated (using cubic splines). In this case the Euler method was very much easier to program than the Runge–Kutta method and was therefore used throughout, with a suitably large number of mesh points, suitably clustered near the free surface. Because of the theorem proved in §4.1, we made no *a priori* assumption about the value of σ_i; like Γ, this quantity was computed as an eigenvalue. In all deep-chamber cases, for every non-zero value of k the corresponding value of σ_i was also non-zero. In many cases, however, the corresponding value of Γ decreased as k was decreased and it was inferred that k_c would be zero, the corresponding values of Γ_c and σ_{ic} (apparently zero) being obtained by extrapolation (see figure 10 below; the numerical problem became singular in the limit $k \to 0$, $\sigma_i \to 0$). However, there was a range of parameters for which k_c (and hence σ_{ic}) was indeed non-zero. Complete details of the numerical method are again given in Hillesdon (1994).

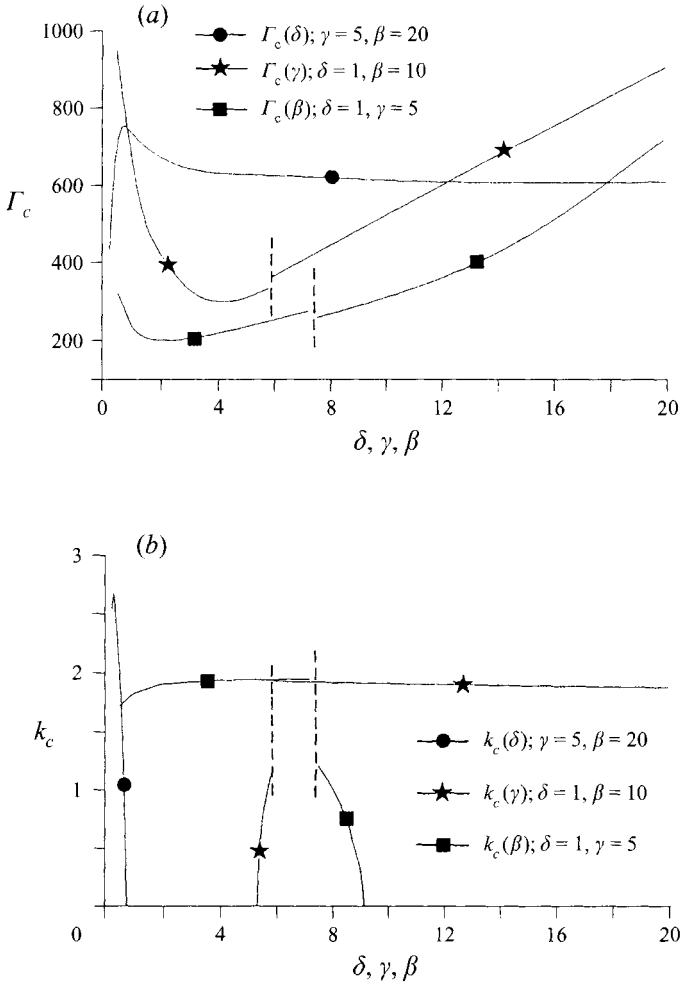

FIGURE 7. (*a*) Computed values of Γ_c, and (*b*) corresponding values of k_c, for cases where δ, γ and β are independently varied. Both shallow- and deep-chamber cases are shown; the vertical dashed lines indicate where the parameter values coincide with the transition line.

4.3. *Results and discussion*

As for a shallow chamber, the values of the parameters β, γ and δ are independently varied and the corresponding values for Γ_c and k_c are determined. It will be of particular interest to examine cases in which the values of γ and β are close to the transition curve (1.41) between shallow- and deep-chamber examples, since one might expect consistency as that curve is approached from either side. Each deep case requires numerical solution of the initial value problem, so that the values of α_c, z_c and the cell concentration below $z = z_c$ are known in the steady state.

Figure 7(*a*) shows how the value of Γ_c varies when δ, γ and β are independently varied, the other parameters being fixed at the quoted values. Figure 7(*b*) shows the corresponding values of k_c for these cases. The vertical dashed lines indicate where the parameter values coincide with the shallow/deep chamber transition.

Several aspects of the results are of interest. First, there appears to be a slight discrepancy between the computed values of Γ_c, and a substantial discrepancy for k_c, as the transition is approached from the shallow- or deep-chamber areas of parameter

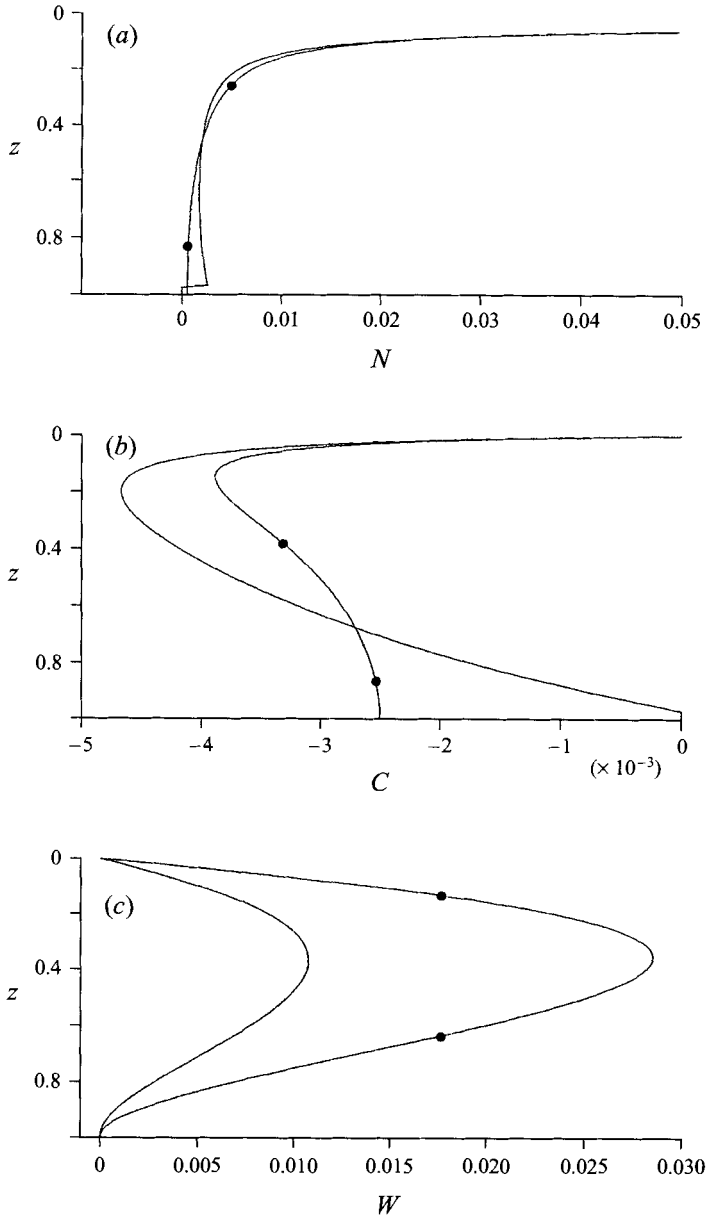

FIGURE 8. Illustration of the different characteristics of the (*a*) N_r, (*b*) C_r, (*c*) W_r perturbation profiles corresponding to the values of Γ_c and k_c for deep ($\gamma = 5.8$, ——) and shallow ($\gamma = 5.952$, —●—) chamber cases close to the transition line ($\delta = 1$, $\beta = 10$).

space. A possible source of error lies in the fact that the shallow-chamber equations are not uniformly valid as the transition is approached, because the perturbation must be taken smaller and smaller to prevent the occurrence of negative values of θ, since at transition the steady-state value of θ is zero at $z = 1$. To illustrate this point we compare the real parts of the N, C, W solutions for a deep-chamber example near to the transition curve ($\delta = 1$, $\gamma = 5.8$, $\beta = 10$) with the N, C, W solutions for a suitable shallow-chamber case that also lies very close to this curve ($\delta = 1$, $\gamma = 5.952$, $\beta = 10$). The comparison is shown in figure 8. Apart from the discontinuous jump in the N

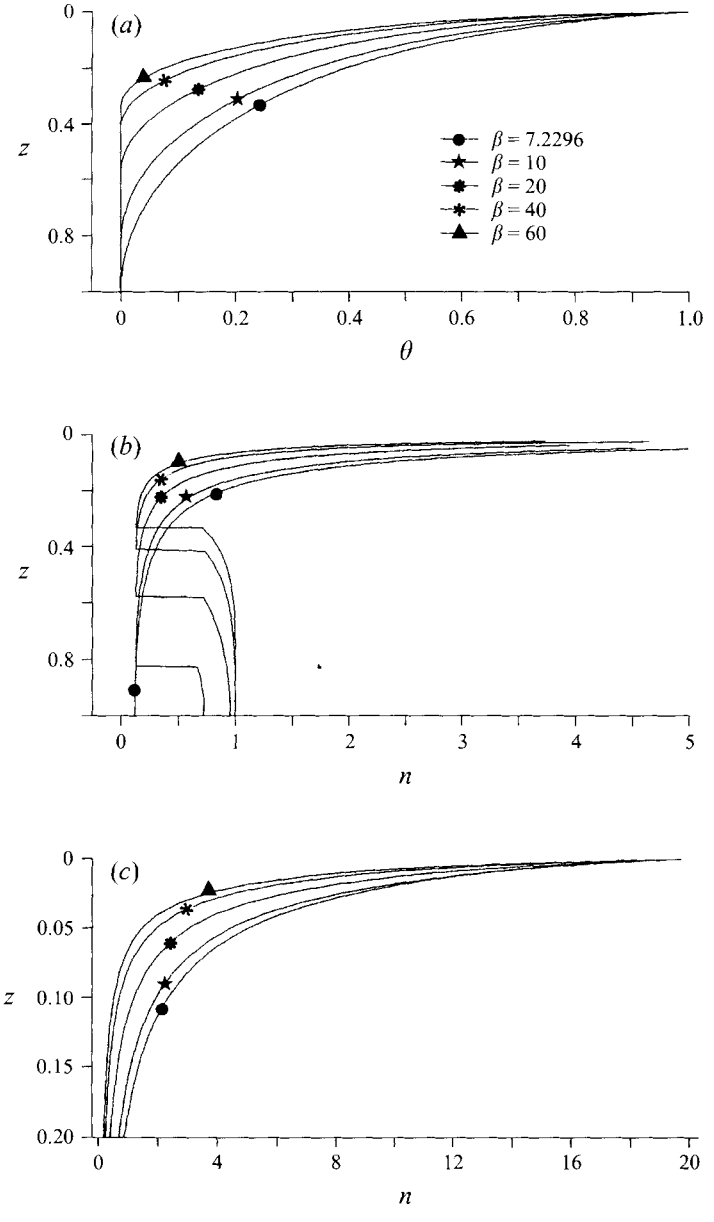

FIGURE 9. Steady-state dimensionless (*a*) oxygen and (*b*, *c*) cell concentration profiles corresponding to $\delta = 1$, $\gamma = 5$, $\beta = 7.2296$, 10, 20, 40, 60; (*b*) and (*c*) show the cell concentration profiles in the main body of the chamber and in the cell boundary layer respectively.

distribution in the $\gamma = 5.8$ case, the most striking difference lies, as expected, in the C distributions. Although the zero-cell-flux condition at $z = 1$ is satisfied for the case with $\gamma = 5.952$, the constraint on the sign of θ will not be. As a result, there is a noticeable difference between the N and W profiles, and hence the values of Γ_c and k_c. The above comments, together with the large jump in the value of k_c at transition (figure 7*b*), suggest that the limit $z_c \to 1$ is singular and requires additional analysis in the future.

Figure 7(*b*) shows that there is rather a limited range of deep-chamber parameter values for which the critical wavenumber is non-zero and the instability is necessarily

oscillatory. Indeed, the numerical results for σ_{ic} show that the instability becomes non-oscillatory again ($\sigma_{ic} = 0$) when k_c goes to zero, although that is not required by the result proved in §4.1. For each example considered, the value of σ_i attains a maximum at a particular wavenumber k, not usually equal to k_c. As the transition is approached from the deep-chamber region, $z_c \to 1$ and we find that the maximum value of $\sigma_i(k)$ decreases to zero. This is to be expected because the depth of the stable region becomes significantly smaller than that of the unstable region and so the oscillations induced by the interaction of these regions will also diminish.

Another important feature of the results that is not seen in figure 7 is that for each set of parameters (β, γ, δ) the mode of disturbance depends significantly on the wavenumber k. In all of the cases considered, as the wavenumber of the disturbance increases then so too does the mode of the vertical velocity field $W(z)$. How often the mode increases depends on several factors, but it appears that the extent of the cell boundary layer and the position of the cut-off point are the most important (see below).

The effect of independent changes in the parameter values for the above examples is discussed in greater detail in the following sections.

4.3.1. *Vary* β; $\delta = 1$, $\gamma = 5$

The results for deep chambers in figure 7 indicate that as the value of β increases (oxygen consumption increasing relative to oxygen diffusion, equivalent to a depth increase) the critical Rayleigh number, Γ_c, also increases. In addition, the corresponding wavenumber k_c is non-zero in a small region close to the transition line given by (1.41), but rapidly diminishes to zero as β is increased. The steady-state cell concentration profiles for selected examples are shown in figure 9.

Figure 10(*a*) shows the curve $\Gamma(k)$ for the shallow- and deep-chamber cases corresponding to $\beta = 7.2296$ and $\beta = 7.5$ respectively. The curves are almost identical except for wavenumbers smaller than 2, where the values of Γ differ significantly. This may be because for this range of values the corresponding dimensional wavelength, λ^*, becomes relatively high compared with the depth of the chamber h, so the disturbances will penetrate to the bottom and the presence of the stable region will have a greater effect.

For cases where $\beta \geqslant 10$, the curves $\Gamma(k)$ are shown in figure 10(*b*). The qualitative behaviour is the same in each case: as k increases from zero the Rayleigh number Γ increases steadily upwards from its minimum value. As β increases so too does the value of Γ_c, in rough proportion to $\beta^{3/2}$ (note that $\beta \propto h^2$ and $\Gamma \propto h^3$). A different possible scaling for Γ is discussed in §5.

The dependence of σ_i on k for $\beta = 10$, 20, 40, 60 is shown in figure 10(*c*). The frequency of oscillation corresponding to a particular wavenumber is greatest in the $\beta = 60$ case, for $k > 2$. This behaviour is presumably related to the change with β of the stable part of the steady-state density distribution (figure 9).

For $\beta = 10, 20$ the motion of the fluid at the critical Rayleigh number consists of a single convection cell. Thus the motion initiated in the upper unstable zone penetrates through the stable layer to reach the lower boundary. In such cases we would expect that, as the convection develops, the whole chamber will become involved in the motion – and the stable zone will lose its identity. This has been observed experimentally. The observed initial motion presumably has a wavenumber equal to the most unstable wavenumber, k_m, corresponding to the actual, supercritical value of Γ. Even when $k_c = 0$ we would not expect k_m to be zero (cf. Hill *et al.* 1989), except when Γ is only infinitesimally greater than Γ_c. In figure 11(*a*) we plot the streamlines

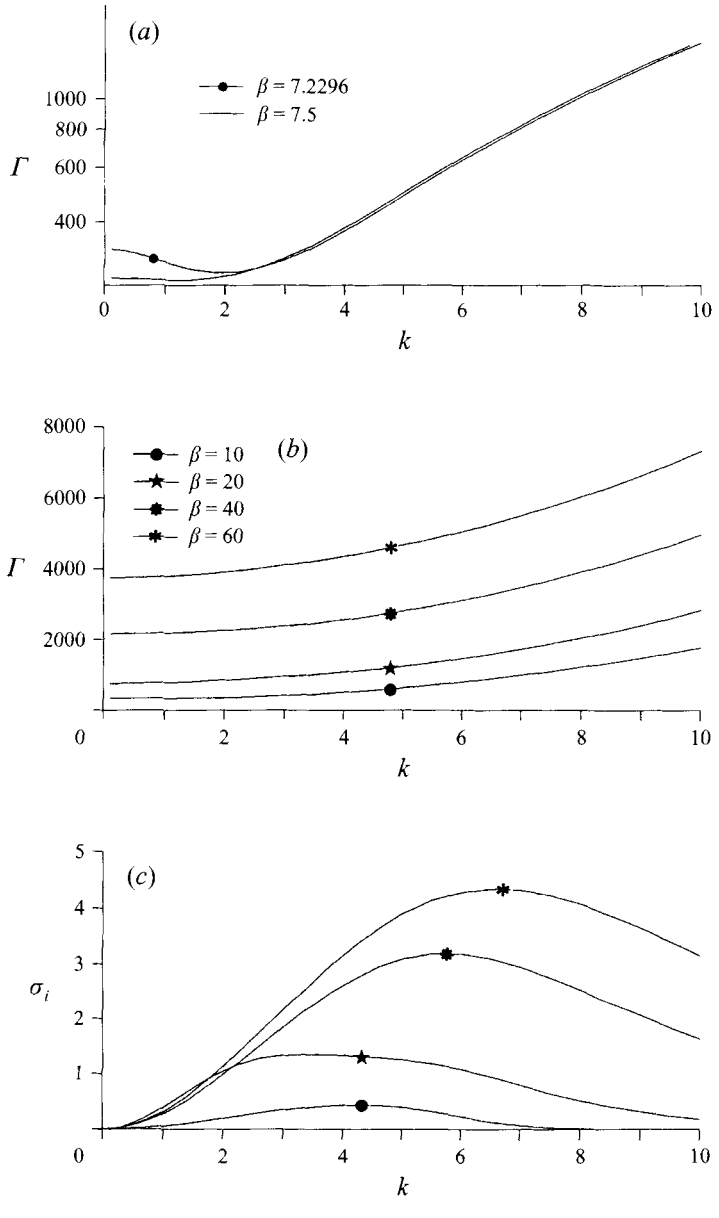

FIGURE 10. (*a*) Comparison of the curves $\Gamma(k)$ for the shallow-chamber case where $\beta = 7.2296$ and the deep-chamber case where $\beta = 7.5$. (*b*) The curves $\Gamma(k)$ and (*c*) $\sigma_i(k)$ corresponding to different values of β. For each figure, $\delta = 1$, $\gamma = 5$.

corresponding to $\Gamma = \Gamma_c$, $k = 0.1$, to give some idea of the flow patterns at the onset of instability when $\beta = 20$.

The distance of penetration into the stable region appears to depend on the value of β. For high enough values of β the fluid motion at the critical Rayleigh number is of mode 2, i.e. consists of two convection cells. Viscous forces exerted by the motion in the upper unstable region drive counter-rotating cells within the lower stable region, and the primary cells penetrate only part way into the stable region. The streamlines for $\beta = 60$, $\Gamma = \Gamma_c$ and $k = 0.1$ are shown in figure 11(*b*). The horizontal dashed line

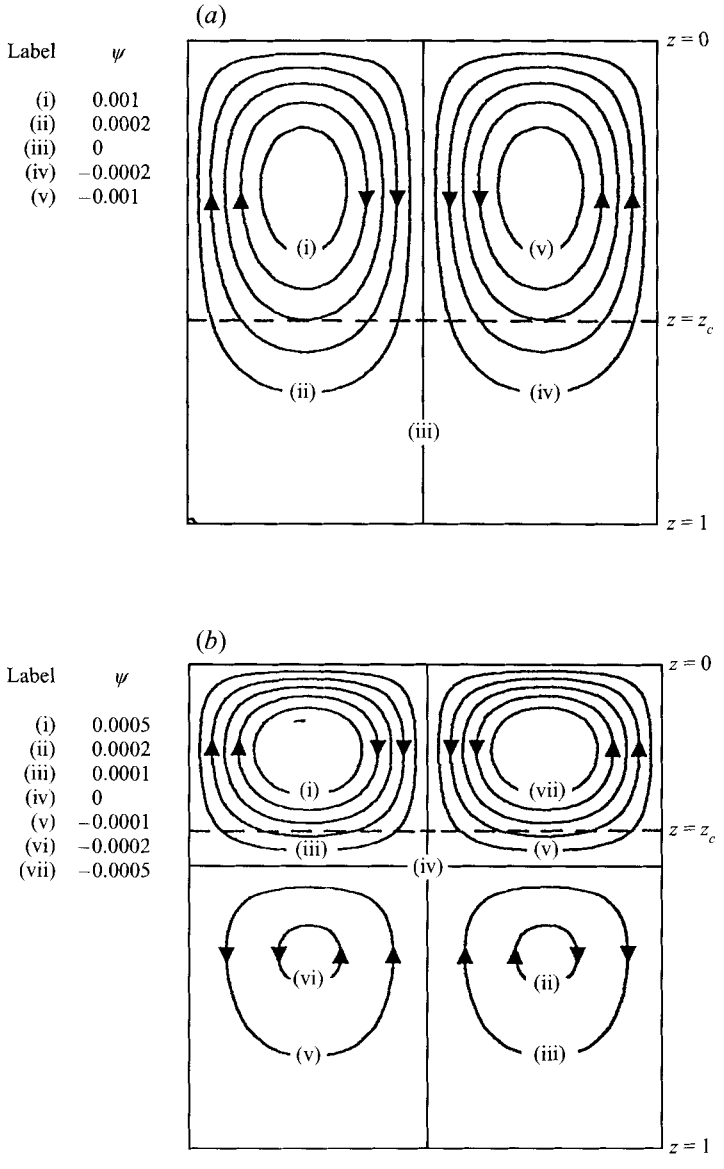

FIGURE 11. Streamlines at the onset of instability for the cases $\delta = 1$, $\gamma = 5$, $\beta = 20, 60$. In (*a*) $\beta = 20$, $\Gamma = 729 \approx \Gamma_c$ and $k = 0.1$, and in (*b*) $\beta = 60$, $\Gamma = 3756 \approx \Gamma_c$ and $k = 0.1$. The horizontal dashed lines show the position of the steady-state cut-off point $z = z_c$. Values of the stream function, ψ, are given in the figure legend.

corresponds to the position of the critical cut-off point $z = z_c$; the upper cells penetrate a dimensionless distance of approximately 0.08 beyond $z = z_c$. The distance of penetration decreases as β increases. From an experimental point of view, in this situation the stable region could still be visibly distinguished from the unstable region above, and this type of behaviour has also been observed experimentally for sufficiently deep chambers.

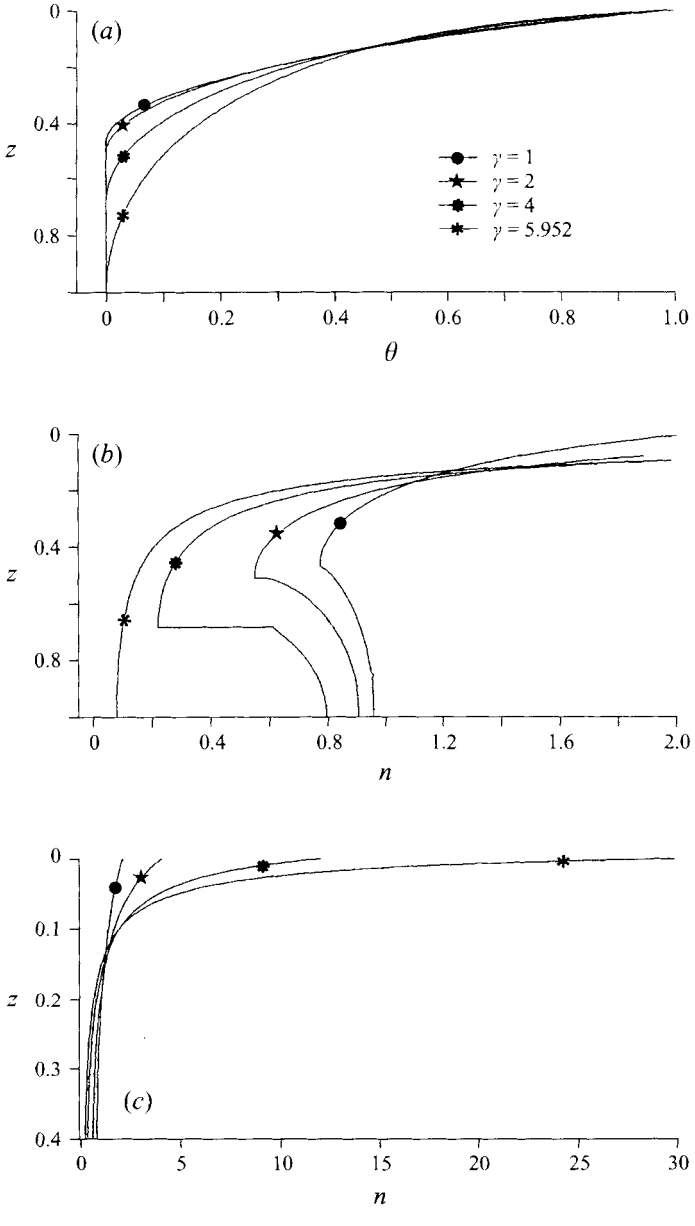

FIGURE 12. Steady-state dimensionless (*a*) oxygen and (*b*, *c*) cell concentration distributions for the cases where $\delta = 1$, $\beta = 10$ and $\gamma = 1, 2, 4, 5, 5.952$. The cell concentration profiles in the main body of the chamber and in the cell boundary layer are shown in (*b*) and (*c*) respectively.

4.3.2. *Vary* γ; $\delta = 1$, $\beta = 10$

Figure 7(*a*) shows that for γ corresponding to a deep chamber ($\gamma \leqslant 5.8$ with $\delta = 1$ and $\beta = 10$) an increase in γ (directed cell swimming increasing relative to diffusive swimming) leads initially to a fall in Γ_c, which reaches a minimum of ≈ 300 when $\gamma \approx 4$. Qualitatively, this behaviour is consistent with the change in cell distribution associated with increased values of γ (see figure 12) as the most unstable deep-layer distributions are expected to occur when the density gradient is steepest. However, for $\gamma > 4$ the value of Γ_c increases with γ. This behaviour is analogous to that observed

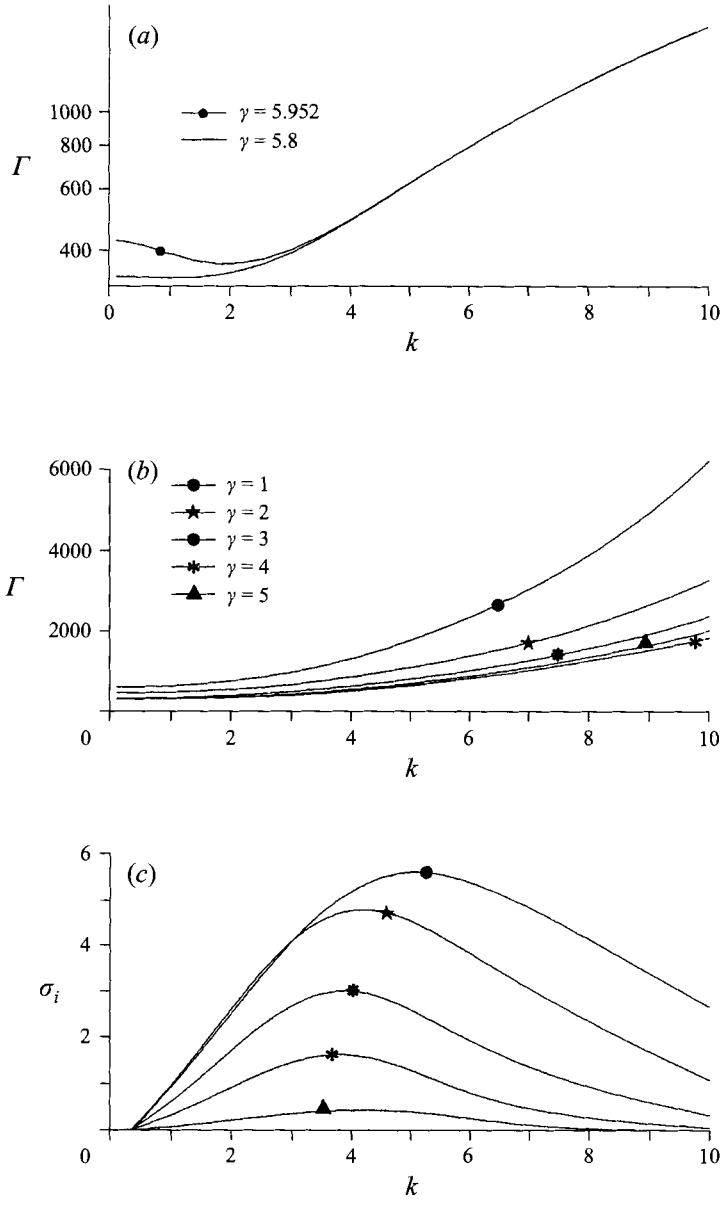

FIGURE 13. (*a*) Comparison of the curves $\Gamma(k)$ for the shallow-chamber case where $\gamma = 5.952$ and the deep-chamber case where $\gamma = 5.8$. (*b*) The curves $\Gamma(k)$ and (*c*) $\sigma_i(k)$ corresponding to different values of γ. For each figure, $\delta = 1$, $\beta = 10$.

in the shallow-chamber case as $\gamma\beta$ is increased; as in that case it may be attributable to an inappropriate definition of Γ (see §5).

As when β is varied, the solutions give non-zero values of k_c (and σ_i) only when γ takes a value close to the deep–shallow transition. Figure 13(*a*) shows the curves $\Gamma(k)$ for the cases $\gamma = 5.8$ and $\gamma = 5.952$, so that the difference in behaviour between the deep and shallow chambers can be compared. Again there is close agreement between the two values of Γ for wavenumbers higher than a particular value, which for this case is $k \approx 3$. Although not graphically obvious, there is in fact a minimum at $k \approx 1.1$ for

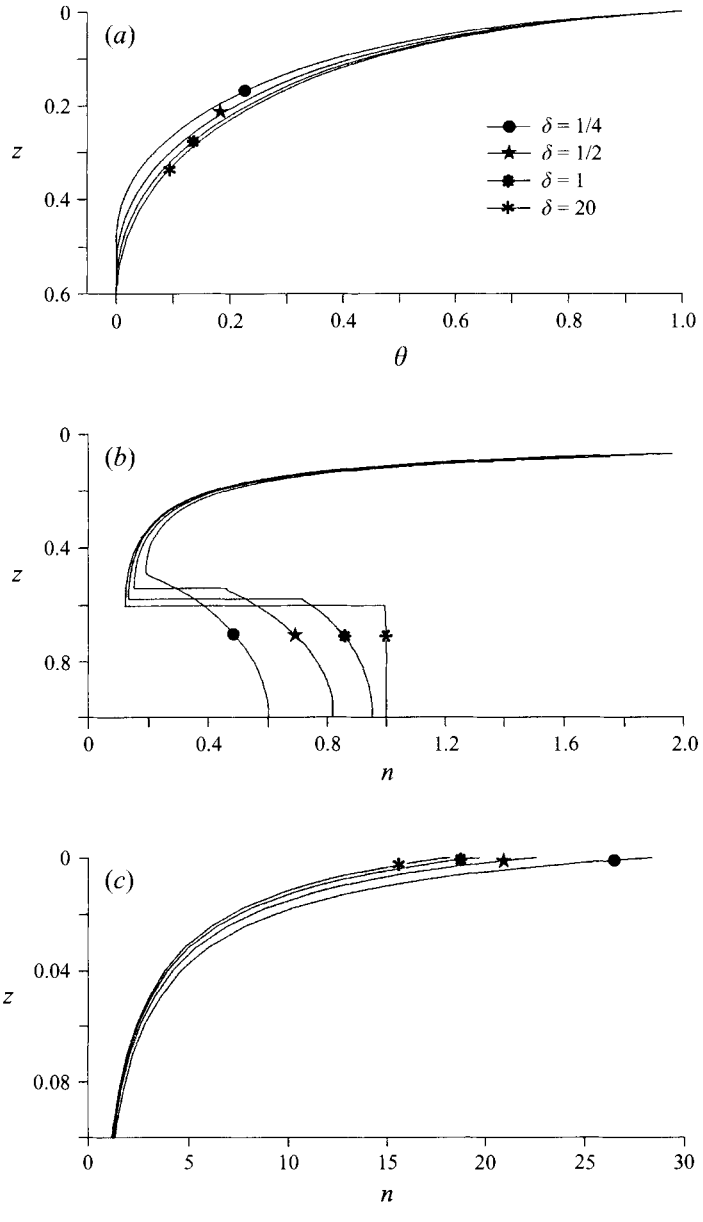

FIGURE 14. Steady-state dimensionless (*a*) oxygen and (*b*, *c*) cell concentration distributions for the cases where $\gamma = 5$, $\beta = 20$, and $\delta = 1/4, 1/2, 1, 20$. The cell concentration profiles in the main body of the chamber and in the cell boundary layer are shown in (*b*) and (*c*) respectively.

the $\gamma = 5.8$ case. The curves $\Gamma(k)$ for $\gamma = 1, 2, 3, 4, 5$ are shown in figure 13(*b*). Note that the variation in γ appears to have a more significant effect on the gradient of the curve $\Gamma(k)$ than on the initial point of the curve, unlike the variation in β for which the converse is true. The curves $\sigma_i(k)$ for these cases are shown in figure 13(*c*); as $z_c \to 1$ the curves broaden out and the peak value falls. This is because the unstable region is significantly deeper than the stable region below and, therefore, results will become more like those obtained in the shallow-chamber case.

For all of the values of γ considered the most unstable mode of disturbance

corresponds to a single convection cell occupying the entire chamber. When the position of the critical cut-off point is close to the upper surface, the extent of the cell boundary layer is significantly reduced (since γ is small), as shown in figure 12(*c*) (to be compared with figure 9*c*). Therefore the energy available to produce a counter-rotating cell, which depends on the density gradient above the cut-off point, will presumably be much lower. In addition, the cell concentration at the critical cut-off point is continuous and the discontinuity in cell concentration gradient is significantly reduced for such cases. Therefore the stabilizing effect on any instability initiated in the upper region will be low and the most dominant disturbance is of mode 1.

4.3.3. *Vary* δ; $\gamma = 5$, $\beta = 20$

Perhaps the most interesting and complex behaviour occurs as the value of δ is independently varied. In a deep chamber, unlike a shallow one, the steady-state cell and oxygen concentration distributions depend on δ. These distributions are shown for various values of δ in figure 14(*a–c*). As the value of δ increases (cells diffusing less vigorously than oxygen), the surface layer becomes less packed with cells and the lower stable region reduces slightly in depth but increases in average cell concentration so that the density discontinuity increases; for $\delta = 20$ the cell concentration below the cut-off point is close to the initial cell concentration, $n = 1$. The curves $\Gamma(k)$ corresponding to these cases are shown in figures 15(*a*) and 15(*b*). The qualitative and quantitative behaviour of these curves changes significantly with the value of δ; for small enough values of δ the existence of a non-zero critical wavenumber is clearly evident. The curves $\sigma_i(k)$ for $\delta = 1/4, 1/2, 1, 20$ are shown in figure 15(*c*). It can be seen that a lower maximum value of $\sigma_i(k)$ (dimensionless frequency) is associated with a larger value of δ and hence with a greater discontinuity in the cell concentration at the interface. This is rather surprising and indicates that other factors affect the magnitude of $\sigma_i(k)$. Moreover, additional results show that $\sigma_m = \max[\sigma_i(k)]$ (say) starts to fall when δ decreases below 0.3; these are cases for which the cell concentration at $z = z_c$ is continuous, so other factors must determine the value of σ_m in this instance.

For convenience, we describe how the results change as δ is decreased from 20, above which they are virtually independent of δ. Figure 7(*a*) shows that as δ is reduced from 20 to 0.67, the critical Rayleigh number increases. On the other hand, the steady-state cell concentration profile for these cases looks more unstable as δ is decreased, again suggesting that a more appropriate definition of Rayleigh number is required. In this range of values, the critical Rayleigh number occurs at $k = 0$ (where $\sigma_i = 0$) and the disturbance is mode 1, except between $\delta = 0.8$ and $\delta = 0.67$, where it is mode 2. When δ is reduced below 0.67, the value of Γ_c starts to decrease again, the value of k_c becomes non-zero (and $\sigma_i \neq 0$), and the corresponding instability remains initially at mode 2. The critical wavenumber increases rapidly to attain its maximum value, $k_c \approx 2.7$, when $\delta = 0.3$; the mode of the critical solution returns to 1 at this value of δ. It is interesting to note that in this case ($\delta = 0.3$), unlike the others considered so far, the mode of the motion does not initially increase with k; for $k = 0.1$ to $k = 1.8$ the solution is mode 2, for $1.8 < k \leqslant 3.4$ the mode falls to 1, and for $k > 3.4$ the mode of the solution increases again. As δ is further reduced, the range of wavenumbers corresponding to mode 1 solutions increases, to the extent that the behaviour observed in the $\delta = 0.3$ case no longer occurs when $\delta = 0.2$. Instead the mode increases intermittently from 1 as k is increased – as in the cases where γ and β are independently varied.

The change in form of the steady-state cell concentration profile as δ changes value is presumably responsible for the wide range in behaviour of the solutions. The cell

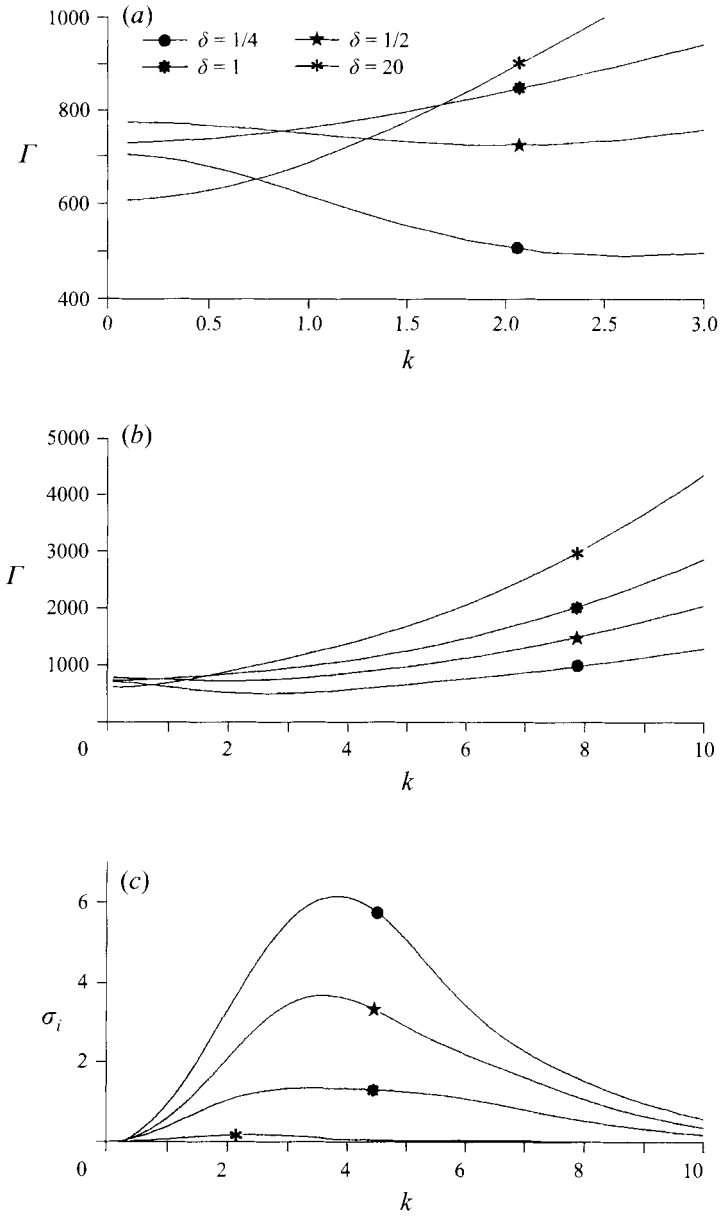

FIGURE 15. (*a*) Comparison of the $\Gamma(k)$ curves over the range, $0 < k \leqslant 3$, for different values of δ. (*b*) The curves $\Gamma(k)$ and (*c*) $\sigma_i(k)$ corresponding to different values of δ, over the range $0 < k \leqslant 10$. For each figure, $\gamma = 5$, $\beta = 20$.

profiles shown in figure 14(*b*) show that the greater the discontinuity in the steady-state cell concentration *gradient* $\mathrm{d}n/\mathrm{d}z$, the more likely is the mode of the solution to be greater than 1. A dependency on the gradient is not surprising because equation (2.9*b*) shows that the $W(z)$ profile in region 2 is strongly influenced by $\mathrm{d}n/\mathrm{d}z$. The hypothesis is certainly consistent with the examples considered so far. When $\delta = 20$, the jump in the value of $\mathrm{d}n/\mathrm{d}z$ is quite small ($\approx 1.14 \times 10^{-2}$) and the mode of the $W(z)$ profile at Γ_c is 1, whereas when $\delta = 0.5$ the jump in value is significantly higher (≈ 1.34) and the critical solution is mode 2. When $\delta = 0.2$, the magnitude of the discontinuity in $\mathrm{d}n/\mathrm{d}z$

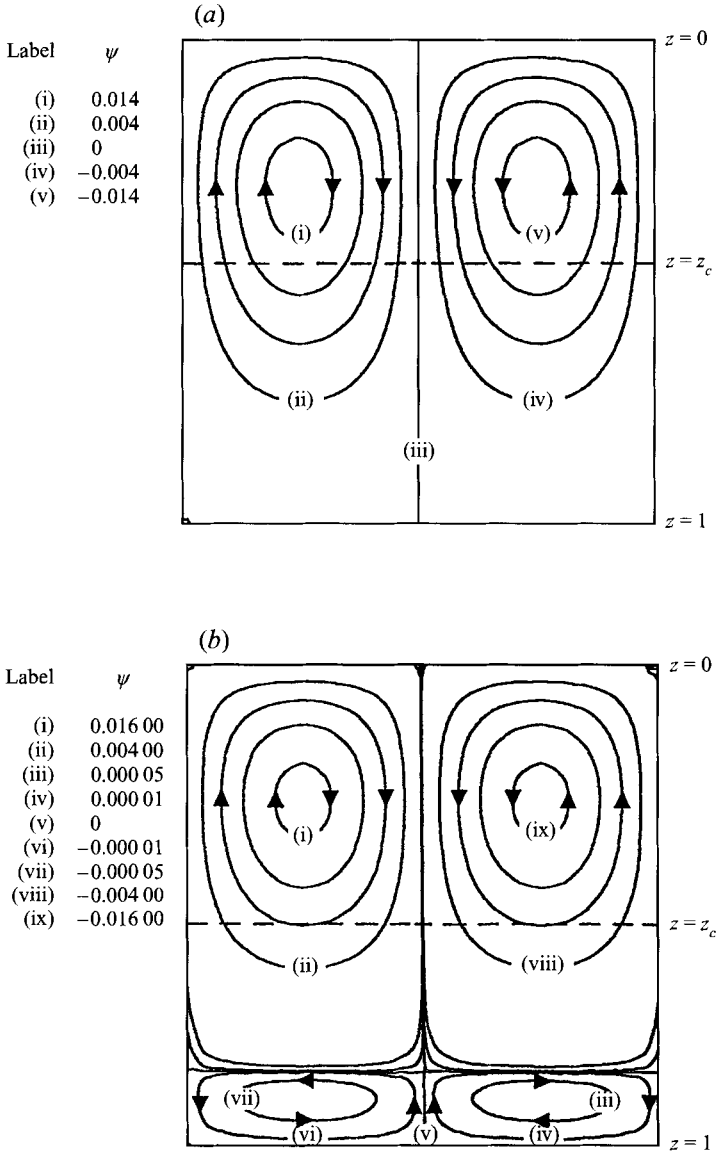

FIGURE 16. Streamlines at the onset of instability for the cases $\delta = 0.2$, 0.5, $\gamma = 5$, $\beta = 20$. In (*a*) $\delta = 0.2$, $\Gamma = 418 \approx \Gamma_c$ and $k \approx 2.53$, and in (*b*) $\delta = 0.5$, $\Gamma = 723 \approx \Gamma_c$ and $k \approx 1.71$. The horizontal dashed lines show the position of the steady-state cut-off point $z = z_c$. Values of the stream function, ψ, are given in the figure legend.

is smaller than that in the $\delta = 0.5$ case and the solution is again of mode 1. To highlight this difference in behaviour the streamlines for the cases with $\delta = 0.2$ and $\delta = 0.5$ are shown in figures 16(*a*) and 16(*b*) respectively.

Another important feature of the results is the behaviour of the critical wavenumber. In particular, what is the mechanism by which a zero critical wavenumber is selected in some cases but not in others? To attempt an answer it is first useful to consider again the shallow-chamber problem, in which non-zero critical wavenumbers were obtained in all cases. We investigate whether this result would still be true if the form of the governing equations were altered. In particular, we look at the effects on the value of

k_c caused by removing (i) the term associated with oxygen consumption by the cells, and (ii) the terms associated with cell swimming. In each case the steady-state cell and oxygen concentration profiles obtained from the solution of the full problem are used. For (i), the neutral curves change considerably; the critical wavenumber falls in each case considered and the rate of change of Γ as $k \to 0$ is significantly reduced. This behaviour closely resembles that obtained in the full solution of the deep-chamber problem for examples close to the transition line. In (ii), the shallow-chamber problem gives $k_c = 0$ in all cases considered (as expected from the similarity to thermal convection with insulating boundaries: Chapman & Proctor 1980). Therefore, it appears plausible that in the deep-chamber linear instability problem, the loss of the consumption and swimming terms in the governing equations for the stable region (where $\theta = 0$) may contribute to the observed behaviour.

The reasons why the critical wavenumber suddenly becomes non-zero when $\delta \leqslant 0.67$ are not obvious. The result may be related to the shallow-chamber results in which k_c falls as δ rises (table 3 and figure 5), though in that case k_c is never zero.

The dependence of the critical wavenumber on the precise form of the governing equations and boundary conditions has become apparent in other pattern formation problems. In a model developed by Childress, Levandowsky & Spiegel (1975) for bioconvection in suspensions of the ciliated protozoan, *Tetrahymena pyriformis*, zero critical wavenumbers were predicted for all parameter values. However, in a later model by Hill *et al.* (1989), for bioconvection in suspensions of algae, the governing equations were similar to those in the Childress case but with additional terms to account for gyrotaxis. This problem typically gives non-zero critical wavenumbers.

5. Further discussion: alternative definitions of the Rayleigh number

The solution of the linear instability problem for both shallow and deep chambers shows that in cases where a significant cell boundary layer forms in the steady state ($\gamma\beta \gg 1$) the computed value of Γ_c, which should be an indicator of the relative instability of a particular suspension, is not well correlated with the density distribution (defined by the values of β, γ, δ). We believe that the problem lies with the definition (1.20) of the Rayleigh number, Γ, proportional to $N_0 h^3$, where N_0 is the mean (initial) cell concentration and h is the chamber depth. In boundary layer cases a more appropriate definition would replace N_0 by N_s, a measure of the concentration difference across the layer which we can take to be the concentration at the upper surface, and replace h by L, a scale for the layer thickness. Other authors in this field have proposed similar alternative definitions, e.g. Hill *et al.* (1989), and Childress *et al.* (1975). The problem therefore is to determine an appropriate sub-layer definition, given the form of the steady-state cell distribution. The shallow- and deep-chamber definitions will therefore differ, and are considered separately.

5.1. *Shallow-chamber definition*

For $\gamma\beta \gg 1$, an appropriate length scale L is given by HPK as

$$L = 2h/\gamma\beta, \tag{5.1}$$

and the surface cell concentration N_s (cells cm^{-3}) is given by

$$N_s = N_0 \left(\frac{A_1^2}{\gamma\beta}\right) \sec^2(\tfrac{1}{2}A_1) \sim N_0 \frac{\gamma}{2}\beta \tag{5.2}$$

as $\gamma\beta \to \infty$ (see (1.32) and (1.33)). Consequently, if we write

$$\tilde{\Gamma} = \frac{v\alpha N_s g}{\nu D_{N0}} L^3,$$

we see from (1.20) that

$$\tilde{\Gamma} = \left(\frac{4}{\gamma^2\beta^2}\right)\Gamma. \tag{5.3}$$

The appropriateness of $\tilde{\Gamma}$ as a definition of the Rayleigh number in the limit $\gamma\beta \gg 1$ can also be verified directly from the governing equations. After N and C have been eliminated, equations (2.5*a–c*), with $\sigma = 0$, can be manipulated to obtain the following single equation for W:

$$\left(\mathscr{L}\left(\mathscr{L} - \gamma\frac{\mathrm{d}\theta}{\mathrm{d}z}\frac{\mathrm{d}}{\mathrm{d}z} - 2\gamma\beta n\right) - \gamma\beta\frac{\mathrm{d}n}{\mathrm{d}z}\frac{\mathrm{d}}{\mathrm{d}z}\right)\mathscr{L}^2 W$$

$$= \Gamma\frac{\mathrm{d}n}{\mathrm{d}z}k^2\left(\mathscr{L} + \frac{\gamma}{\delta}\frac{\mathrm{d}\theta}{\mathrm{d}z}\frac{\mathrm{d}}{\mathrm{d}z} + \frac{\gamma}{\delta}\beta n + \left(1+\frac{1}{\delta}\right)\left[\gamma^2\left(\frac{\mathrm{d}\theta}{\mathrm{d}z}\right)^2 + 4\gamma\beta n\right]\right)W, \tag{5.4}$$

where $\mathscr{L} = \mathrm{d}^2/\mathrm{d}z^2 - k^2$. In the boundary layer a suitable scaling for z is

$$Y = \gamma\beta z/2, \tag{5.5}$$

and, given that the horizontal lengthscale of the disturbance should also be L, the wavenumber should be re-scaled such that

$$\tilde{k} = 2k/\gamma\beta. \tag{5.6}$$

Then, using the boundary layer representations of the steady-state cell and oxygen concentrations (from HPK), we obtain

$$\left\{\tilde{\mathscr{L}}\left\{\tilde{\mathscr{L}} + \frac{2}{1+Y}\frac{\mathrm{d}}{\mathrm{d}Y} + \frac{4}{(1+Y)^2}\right) + \left(\frac{4}{(1+Y)^3}\frac{\mathrm{d}}{\mathrm{d}Y} - \frac{8}{\delta\gamma^2\beta^2(1+Y)^2}\right)\right\}\tilde{\mathscr{L}}^2 W$$

$$= -\frac{8\tilde{k}^2\Gamma}{\gamma^2\beta^2(1+Y)^3}\left(\left(1+\frac{1}{\delta}\right)\frac{\mathrm{d}^2 W}{\mathrm{d}Y^2} - \frac{2}{\delta}\frac{\mathrm{d}}{\mathrm{d}Y}\left[\frac{W}{(1+Y)}\right] + 4\left(1+\frac{1}{\delta}\right)\left[\frac{3}{(1+Y)^2} - \tilde{k}^2\right]W\right), \tag{5.7}$$

where $\tilde{\mathscr{L}} = \mathrm{d}^2/\mathrm{d}Y^2 - \tilde{k}^2$, which indicates that the appropriate Rayleigh number for the suspension is indeed as given in (5.3). Figure 17(*a*) shows how $\tilde{\Gamma}_c$ varies with $\gamma\beta\,(\geqslant 1)$ for the cases where $\delta = \frac{1}{2}, 1, 20$. The behaviour of $\tilde{\Gamma}_c$ as $\gamma\beta$ increases is now intuitively reasonable, suggesting that, as the density stratification increases, the suspension becomes more unstable.

Figure 17(*b*) shows the relationship between $\tilde{k}_c$ and $\gamma\beta$. This tells us that the re-scaled wavelength, $\tilde{\lambda}_c$, corresponding to $\tilde{k}_c$, increases as the value of $\gamma\beta$ increases, and does not tend to a constant. Hence the initial spacing of the bioconvection patterns does depend significantly on the chamber depth, and is not determined solely by the characteristics of the boundary layer.

5.2. *Deep-chamber definition*

The definition of an alternative Rayleigh number for deep chambers follows the same procedure as for shallow chambers. The only difference is that we assume that the instability of the system is determined by the nature of the cell distribution only in the region above the cut-off point $z = z_c$.

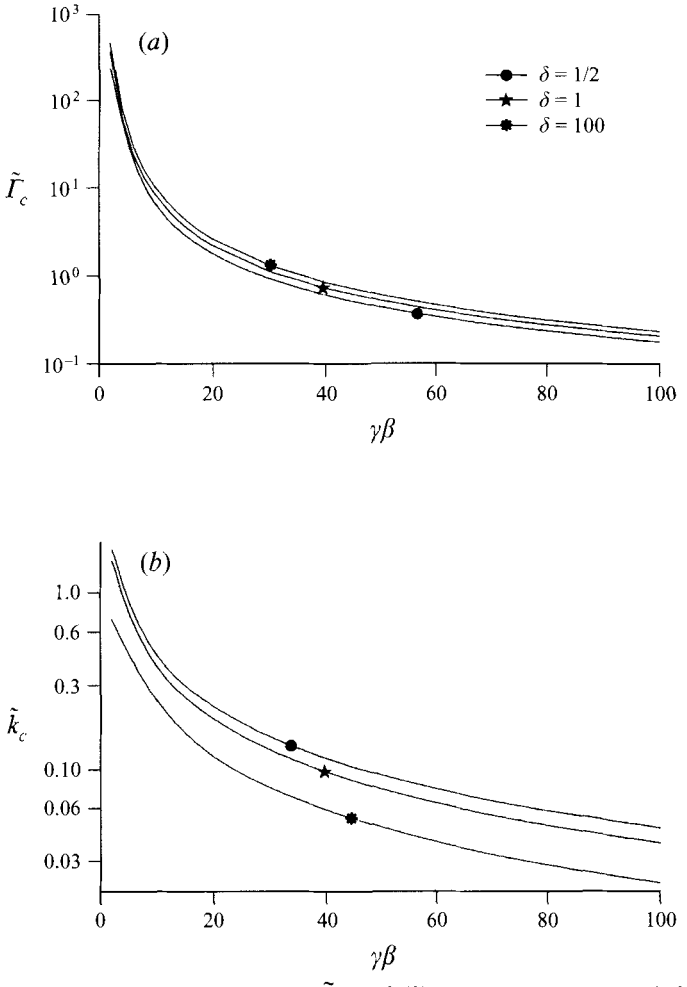

FIGURE 17. (*a*) Re-scaled Rayleigh number, $\tilde{\Gamma}_c$, and (*b*) corresponding re-scaled values of $\tilde{k}_c$, both plotted against $\gamma\beta$, for given values of δ. The behaviour of $\tilde{\Gamma}_c$ as $\gamma\beta$ increases is intuitively reasonable because it suggests that as the density stratification increases, the suspension becomes more unstable. The dependence of $\tilde{k}_c$ on $\gamma\beta$ implies that the initial spacing of the bioconvection patterns depends significantly on the chamber depth h.

As before, N_0 in the definition of Γ is replaced by N_s, which is given by (1.35), for deep chambers with $\gamma\beta \gg 1$, to be approximately

$$N_s \approx \tfrac{1}{2}\gamma\beta\alpha_c^2 N_0. \tag{5.8}$$

In addition, the density stratification that drives the instability is confined to the region $0 \leqslant z \leqslant z_c$ and so for non-boundary-layer cases a more appropriate definition of the Rayleigh number would be

$$\hat{\Gamma} = \left(\frac{N_s \alpha g v}{D_{N0}\nu}\right) z_c^3. \tag{5.9}$$

However, when $\gamma\beta \gg 1$ we must take into account the fact that much of the variation in cell concentration is confined to the small boundary layer region near $z = 0$. The depth of this layer is found from (1.35)–(1.37) to be

$$L = \frac{2}{\gamma\beta\alpha_c^2} z_c, \tag{5.10}$$

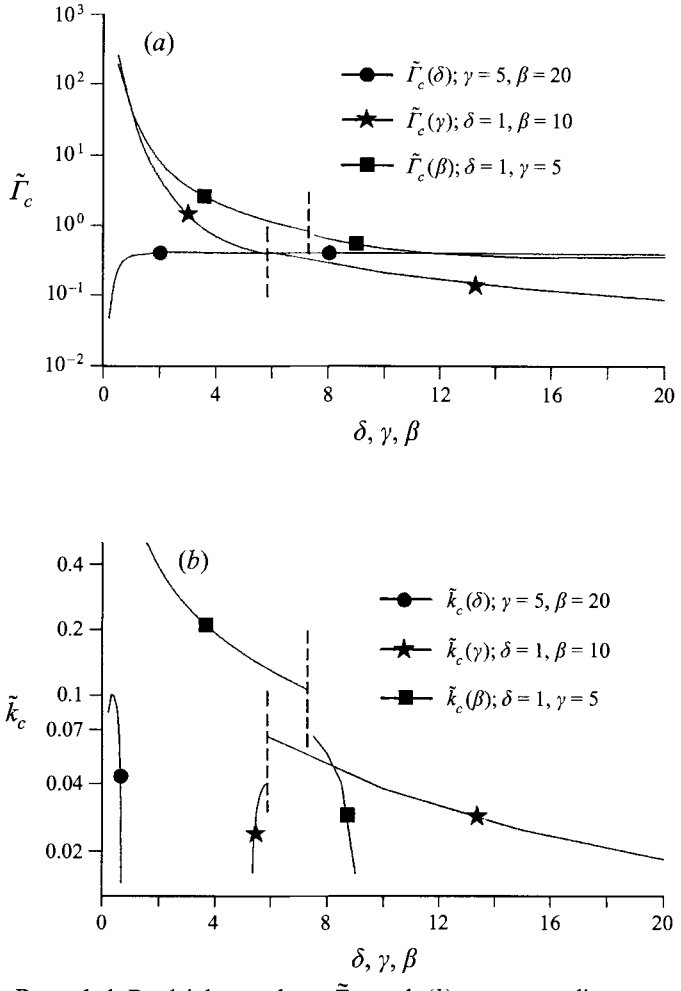

FIGURE 18. (*a*) Re-scaled Rayleigh number, $\tilde{\Gamma}_c$, and (*b*) corresponding re-scaled values of $\tilde{k}_c$, corresponding to the cases where δ, γ, and β are independently varied. Both shallow- and deep-chamber values are shown. The vertical dashed lines correspond to parameter values that coincide with the transition line.

so an appropriate Rayleigh number for the suspension is

$$\tilde{\Gamma} = \left(\frac{2}{\gamma\beta\alpha_c^2}\right)^2 z_c^3 \Gamma. \tag{5.11}$$

Note that the dependence of $\tilde{\Gamma}$ on δ, which is required in deep-chamber cases, comes in via the value of α_c. The deep-chamber definition of $\tilde{\Gamma}$ is consistent with the shallow-chamber definition (5.3) as $z_c \to 1$. The dependence of $\tilde{\Gamma}_c$ on the parameter values for the cases considered is shown in figure 18(*a*). Both shallow- and deep-chamber values are shown. Comparing this figure with figure 7(*a*) we see that the jump in the calculated value of $\tilde{\Gamma}_c$, as one approaches the transition line from the shallow and deep chamber areas of parameter space, is much smaller than that found for Γ_c, suggesting that the re-scaled Rayleigh number is indeed appropriate. The behaviour of the value of $\tilde{\Gamma}_c$ as the parameters δ, γ and β are independently varied is more consistent with the nature of the steady-state cell profiles for these cases. As a result, the curves where γ and β are independently varied no longer possess the local minima observed in figure 7(*a*).

By analogy with the re-scaling of k in the shallow-chamber case, we choose the deep-chamber re-scaling to be

$$\tilde{k} = 2k/\gamma\beta\alpha_c^2. \tag{5.12}$$

The re-scaled values $\tilde{k}_c$ are shown in figure 18(*b*). For clarity, $\tilde{k}_c$ is plotted on a logarithmic scale. The vertical dashed line marks the deep–shallow transition. There is still a marked discontinuity, related to the discontinuous behaviour noted in figure 8.

5.3. *Relation to experiment*

Although we have solved both the shallow- and the deep-chamber linear instability problems, quantitative comparisons with Kessler's experiments (Kessler *et al.* 1994, 1995; HPK) are not possible because accurate values for the upswimming parameter γ and the depth parameter β (and indeed more quantitatively accurate forms for the dependence of the cell diffusivity, cell chemotactic function, and oxygen consumption rate on oxygen concentration) are not available without further more detailed experimental investigation into individual cell behaviour. Nevertheless, certain qualitative aspects of the solution to the deep-chamber problem are found to agree with experimental observation. By independently varying the depth parameter β, we find that at sufficiently large depths the fluid motion at the onset of instability consists of a convection cell occupying the upper unstable zone and a counter-rotating cell lying within the stable zone. The motion in the upper layer actually penetrates part way into the stable region beneath, the depth of penetration appearing to depend on the ratio of the cut-off distance to chamber depth and the nature of the cell stratification above and below the cut-off point. As a result of this fluid motion one would expect most of the cells originally situated in the lower zone to remain there – this behaviour is consistent with experimental observations, although there have been no reports of a counter-rotating eddy in the lower zone. As the depth parameter β is reduced, the motion of the fluid at the onset of instability is predicted to become one consisting of a single convection cell occupying the entire chamber. The stable region of cells will thus participate in the main convective motion and the inert cells will no longer remain in the lower zone, but will be carried upwards, once more receiving oxygen and becoming active. Such behaviour is also consistent with experimental observation.

However, in most experimental demonstrations of instability (see HPK, for example) the first motions to be observed (from the side) consist of plumes descending from the cell-rich layer at the free surface. The streamlines would be concentrated in the plumes and in the surface layer, and not more regularly spaced as in figures 11 and 16. The discrepancy could be a consequence of using inappropriate parameter values, but is more likely to be due to the neglect of the reorientation of cells by shear in the flow, which would cause the cells to swim in towards a descending plume, as already analysed for gyrotactic algae (Pedley & Kessler 1992). After some time, when the flow is necessarily nonlinear, the plumes plunge into the lower zone where they cause mixing.

Our model predicts that immediately above the cut-off point $z = z_c$ the cell concentration and its gradient are characteristically smaller than those found below the cut-off point and hence small perturbations experience a significant gravitational restoring force in this region leading to the generation of gravity waves and hence the oscillatory behaviour predicted by our model for a certain range of parameter values. Such behaviour has yet to be observed experimentally and a further investigation is required.

Quantitative comparisons with experimental results may further require an instability analysis of an evolving cell concentration profile, as it is likely that instability

will set in prior to the steady state being reached. Such an analysis should establish the time at which instability begins and its subsequent growth rate, and is an area of future interest.

Furthermore, when detailed quantitative data concerning individual cell behaviour become available, it may prove useful to consider a more self-consistent model for the cell swimming velocity and cell diffusivity tensor that includes both random and deterministic aspects of cell motion in a probability density function for the cell swimming direction. It would also be necessary to include a term in the cell conservation equation that accounts for the orientation of the cells by shear (rheotaxis or gyrotaxis). This may reveal new aspects of the collective cell behaviour.

Although we have shown that a linear instability analysis can provide a useful qualitative insight into the behaviour of an unstable cell distribution at the onset of instability it is not able to predict the initial planform of the bioconvection patterns. To achieve this at least a weakly nonlinear analysis is required – this is currently being performed.

A.J.H. would like to thank the Science and Engineering Research Council (now EPSRC) for their financial support during this work with a Mathematical Biology Earmarked Studentship. We are grateful to Dr D. R. Moore for providing us with a copy of his computer program (Cash & Moore 1980). We are also particularly grateful to Dr N. A. Hill and Professor J. O. Kessler for their many inputs to this work in the course of numerous fruitful discussions.

REFERENCES

CASH, J. R. & MOORE, D. R. 1980 A high order method for the numerical solution of two-point boundary value problems. *BIT* **20**, 44–52.

CHANDRASEKHAR, S. 1961 *Hydrodynamic and Hydromagnetic Stability*. Oxford University Press.

CHAPMAN, C. J. & PROCTOR, M. R. E. 1980 Nonlinear Rayleigh–Bénard convection between poorly conducting boundaries. *J. Fluid Mech.* **101**, 759–782.

CHILDRESS, S., LEVANDOWSKY, M. & SPIEGEL, E. A. 1975 Pattern formation in a suspension of swimming micro-organisms; equations and stability theory. *J. Fluid Mech.* **63**, 591–613.

HILL, N. A., PEDLEY, T. J. & KESSLER, J. O. 1989 Growth of bioconvection patterns in a suspension of gyrotactic micro-organisms in a layer of finite depth. *J. Fluid Mech.* **208**, 509–543.

HILLESDON, A. J. 1994 Pattern formation in a suspension of swimming bacteria. PhD dissertation, University of Leeds.

HILLESDON, A. J., PEDLEY, T. J. & KESSLER, J. O. 1995 The development of concentration gradients in a suspension of chemotactic bacteria. *Bull. Math. Biol.* **57**, 299–344 (referred to herein as HPK).

KELLER, E. F. & SEGEL, L. A. 1971*a* Model for chemotaxis. *J. Theor. Biol.* **30**, 225–234.

KELLER, E. F. & SEGEL, L. A. 1971*b* Travelling bands of chemotactic bacteria. *J. Theor. Biol.* **30**, 235–249.

KELLER, H. B. 1974 Accurate difference methods for nonlinear two-point boundary value problems. *SIAM J. Numer. Anal.* **11**, 305–320.

KESSLER, J. O. 1989 Path and pattern – the mutual dynamics of swimming cells and their environment. *Comments Theor. Biol.* **1**, 85–108.

KESSLER, J. O., HOELZER, M. A., PEDLEY, T. J. & HILL, N. A. 1994 Functional patterns of swimming bacteria. In *Mechanics and Physiology of Animal Swimming* (ed. L. Maddock, Q. Bone & J. M. V. Rayner). Cambridge University Press.

KESSLER, J. O., STRITTMATTER, R. P., SWARTZ, D. L., WISELEY, D. A. & WOJCIECHOWSKI, M. F. 1995 Paths and patterns: the biology and physics of swimming bacterial populations. In *SEB Symposium 49: Biological Fluid Dynamics* (ed. C. P. Ellington & T. J. Pedley). Cambridge, Company of Biologists.

PEDLEY, T. J., HILL, N. A. & KESSLER, J. O. 1988 The growth of bioconvection patterns in a uniform suspension of gyrotactic micro-organisms. *J. Fluid Mech.* **195**, 223–237.

PEDLEY, T. J. & KESSLER, J. O. 1990 A new continuum model for suspensions of gyrotactic micro-organisms. *J. Fluid Mech.* **212**, 155–182.

PEDLEY, T. J. & KESSLER, J. O. 1992 Hydrodynamic phenomena in suspensions of swimming microorganisms. *Ann. Rev. Fluid Mech.* **24**, 313–358.

STIX, M. 1970 Two examples of penetrative convection. *Tellus* **22**, 517–520.

VERONIS, G. 1963 Penetrative convection. *Astrophys. J.* **137**, 641–663.

ZAHN, J.-P., TOOMRE, J. & LATOUR, J. 1982 Nonlinear model analysis of penetrative convection. *Geophys. Astrophys. Fluid Dyn.* **22**, 159–193.